

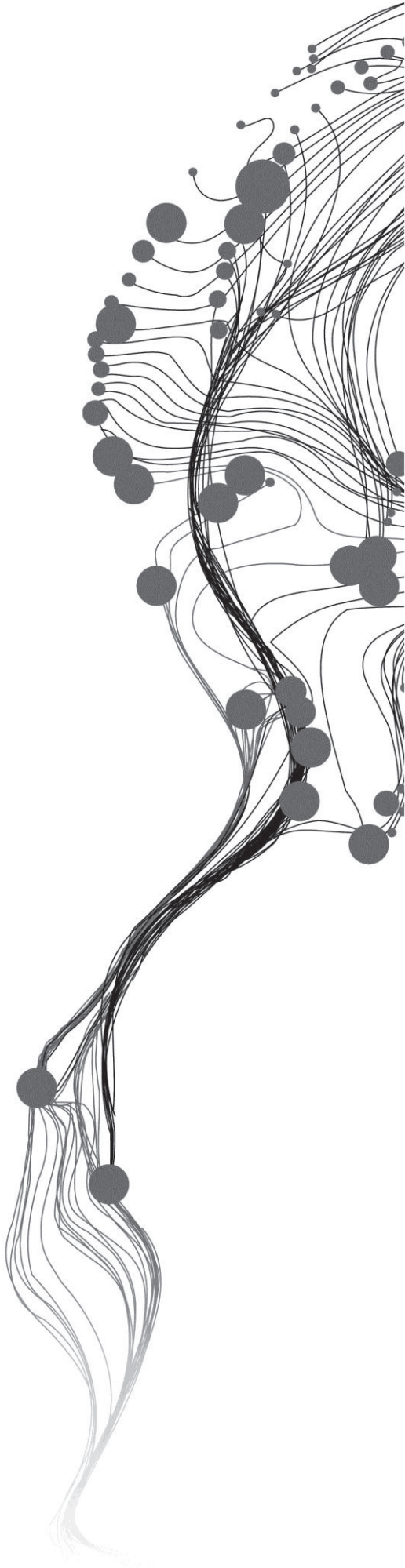
Remote sensing of open water evaporation: A case study of Lake Tana, Ethiopia

BISERAT ASSEGID YITATEKU
February, 2012

SUPERVISORS:

First supervisor: - Dr. Ir. C. van der Tol

Second supervisor:-Dr. Ing. T. H. M. Rientjes



Remote sensing of open water evaporation: A case study of Lake Tana, Ethiopia

BISERAT ASSEGID YITATEKU
Enschede, The Netherlands, February, 2012

Thesis submitted to the Faculty of Geo-Information Science and Earth Observation of the University of Twente in partial fulfilment of the requirements for the degree of Master of Science in Geo-information Science and Earth Observation.

Specialization: Water Resource and Environmental Management

SUPERVISORS:

First supervisor: - Dr. Ir. C. van der Tol

Second supervisor: -Dr. Ing. T. H. M. Rientjes

THESIS ASSESSMENT BOARD:

Dr. Ir. C.M.M. Mannaerts (Chair)

Dr. M.J. Waterloo (External Examiner, Universiteit Amsterdam)

DISCLAIMER

This document describes work undertaken as part of a programme of study at the Faculty of Geo-Information Science and Earth Observation of the University of Twente. All views and opinions expressed therein remain the sole responsibility of the author, and do not necessarily represent those of the Faculty.

ABSTRACT

The diurnal cycle of Lake Tana evaporation is not well understood and requires further study. The main objective of this study is to assess the diurnal cycle of open water evaporation of the Lake Tana using ground measurement and remote sensing data. Remote sensing is used to fill the gap in the data that is created due to the lack of meteorological stations over the water surface and it also improves spatial coverage.

Lake Tana is located in the North-western highlands of Ethiopia at 12°00' N and 37°15' E. The lake has an altitude of 1786m.a.s.l. with a surface area of 3000 km², comprising about 20% of the 15000km² drainage area. The estimation of evaporation from open water is a difficult process in that the necessary meteorological parameters are rarely measured over the water surface and the land based measurements are rendered by the thermal lag between the land and the water surface. By the use of remote sensing data the problem can be solved by obtaining data which covers the area spatially as well as temporally.

In this study four methods are applied to estimate open water evaporation using the components of the energy balance: the latent heat, the net radiation, sensible heat and water heat flux. Firstly, a complete set of in situ data are used to estimate the evaporation and secondly, remote sensing data are used in combination with the in situ data. In both cases the methods are applied and estimates of the hourly evaporation from the lake are computed and assessment on the diurnal cycle of evaporation is made. The result showed that the net radiation and the water heat flux have large effects on the estimate of the hourly evaporation. In the diurnal cycle of evaporation the estimated value ranges from -0.09mm/hour at the night time to a maximum of 1.15mm/hour at the middle of the day. A daily estimate of 3.88mm/day from in situ data and 5.49mm/day for the remote sensing combined with the in situ data is found. The net radiation flux showed a stable negative value during the night and it increases steadily from the morning to the mid- day and then decreases. The hourly estimate of the open water evaporation from the Lake Tana shows the same trend.

Key words: Lake Tana, net radiation, latent heat flux, water heat flux, diurnal cycle of evaporation.

ACKNOWLEDGEMENTS

Above all I thank GOD for his mercy and grace in all my life.

I am deeply indebted to my first supervisor Dr. Ir. C. van der Tol for the supervision, encouragement and guidance he has provided me from the initial to the final level which enabled me to develop an understanding of the subject. Without him it was not possible to complete this thesis.

I am also deeply indebted to my second supervisor Dr. Ing. T. H. M. Rientjes for his critical comments, advice and support that helped me throughout my thesis especially in analyzing the data and interpreting the results.

I am heartily thankful to Ing. Murat Ucer for his kind support and the training he gave me for my field work.

Furthermore, I would like to express my gratitude to the Government and the people of Netherlands and as well to the Netherlands fellowship program (Nuffic) for giving me the opportunity to pursue my MSc study.

I also offer my regards and blessings to all of those who supported me in any respect during my study period.

Last, but by no means least, I thank all my families specially my younger sister Serku for her unreserved support and encouragement.

.

TABLE OF CONTENTS

1. Introduction.....	1
1.1. Background.....	1
1.1. Problem definition.....	1
1.2. Objective(s) and research questions.....	2
1.3. Previous studies.....	2
1.4. Thesis outline.....	2
2. Literature review.....	3
2.1. The process of evaporation.....	3
2.2. The estimation of open water evaporation.....	3
2.3. Diurnal cycle of evaporation.....	3
2.4. The application of remote sensing.....	4
3. study area and data collection.....	5
3.1. Study area.....	5
3.2. In situ data collection.....	8
3.3. Remote sensing data.....	11
3.3.1. MODIS.....	11
3.3.2. The MSG/SEVIRI.....	11
3.3.3. The Land Surface Analysis Satellite Application Facility (LSA SAF).....	13
4. Methodology.....	15
4.1. Estimation of evaporation using in situ data.....	15
4.1.1. The Penman combination equation.....	15
4.1.2. The energy balance method.....	16
4.1.3. The Bowen ratio/Energy balance (BREB) method.....	18
4.1.4. The Bowen ratio method.....	18
4.2. Estimate of evaporation using Remote sensing.....	19
4.2.1. Water heat flux.....	19
4.2.2. Net radiation.....	19
4.2.3. Latent and Sensible heat flux.....	20
4.3. Surface temperature retrieval.....	20
4.3.1. Methods for retrieving LST.....	21
4.3.2. Solar zenith angle and satellite view angle.....	22
5. In situ data analysis and results.....	24
5.1. Water heat flux.....	24
5.2. Net radiation.....	28
5.3. The sensible heat flux.....	29
5.4. Diurnal cycle of evaporation.....	30
5.4.1. The Bowen ratio method.....	30
5.4.2. The Bowen ratio / Energy balance method (BREB).....	30
5.4.3. The Energy balance method.....	31
5.4.4. The Penman combination method.....	31
5.4.5. Comparison of the latent heat flux in the four methods.....	31

6. Remote sensing data analysis and results.....	33
6.1. Net radiation.....	33
6.2. Water heat flux.....	38
6.3. Diurnal cycle of evaporation.....	38
6.4. Comparison of Results.....	41
6.4.1. Comparison of the remote sensing and in situ measurement.....	41
6.4.2. Comparison with previous studies.....	42
7. Conclusions and recommendations.....	45
7.1. Conclusions.....	45
7.2. Recommendations.....	46
List of references.....	47
Anex.....	49
Appendix A: ILWIS Script for water surface temperature retrieval.....	49
Appendix B: ILWIS Script for short wave outgoing.....	50
Appendix C: ILWIS Script for outgoing long wave radiation.....	50
Appendix D: ILWIS Script for Net radiation.....	51
Appendix E: ILWIS Script for Latent heat flux.....	51
Appendix F: ILWIS Script for hourly evaporation.....	52
Appendix G: ILWIS Script for Daily Total evaporation.....	53
Appendix H: Hourly estimate of the component of energy balance(in situ).....	53
Appendix I: Latent heat flux estimated by four methods (in situ).....	54
Appendix J: Comparison of hourly results.....	55

LIST OF FIGURES

Figure 3-1: Location of the study area, Lake Tana (false colour composite of LANDSAT7 image, October 2003)(Abreham Kibret, 2009).....	5
Figure 3-2: Depths of Lake Tana (Wale, 2008).....	6
Figure 3-3: Lake Tana basin (source: Ethiopian ministry of water recourses).	7
Figure 3-4: setting up of instruments on the Lake Tana.....	8
Figure 3-5: setting up of temperature sensors below the Lake surface.....	8
Figure 3-6: The CR-200 Campbell-Scientific data logger, the HOBO 4-channel external data logger and the Thermometer Infrared Testo 830-T2.....	9
Figure 3-7: MSG Data Retriever Window as a plug-in in ILWIS GIS software version 1.3.	13
Figure 5-1: Temperature profile of the water (5 minute interval) (Date: 15/09/2011, 16:40hr-16/09/2011, 17:30hr)	24
Figure 5-2: Hourly water temperature distribution over time for respective measurement depths (Date: 15/09/2011, 17:00hr-16/09/2011, 17:00hr).....	25
Figure 5-3: The average of the hourly change in temperature ($\Delta T/\Delta t$) for a 6hr time period for the respective depth of measurement (Date: 15/09/2011, 18:00hr-16/09/2011, 17:00hr local time).....	26
Figure 5-4: Water heat flux with averaged temperature data (Date: 15/09/2011, 18:00hr-16/09/2011, 17:00hr)	27
Figure 5-5: Different component of the radiation (Date: 15/09/2011, 17:00hr-16/09/2011, 17:00hr)	28
Figure 5-6: Diurnal cycle of net radiation (Date: 15/09/2011, 17:00hr-16/09/2011, 17:00hr).....	29
Figure 5-7: Diurnal cycle of Sensible heat flux (Date: 15/09/2011, 17:00hr-16/09/2011, 17:00hr local time).....	29
Figure 5-8: Diurnal cycle of Bowen ratio (Date: 15/09/2011, 17:00hr-16/09/2011, 17:00hr).....	30
Figure 5-9: Diurnal cycle of latent heat flux with different methods (Date: 15/09/2011, 18:00hr-16/09/2011, 17:00hr).....	31
Figure 6-1: Total albedo of Lake Tana area (a) (15 th of September 2011) and instantaneous net short wave radiation ($W m^{-2}$) (16 th of September 2011 at 10:00 hour local time) (b)	33
Figure 6-2: The incoming and outgoing short wave radiation from the remote sensing data (from 15 th of September 2011 at 18:00hr to 16 th of September 2011 at 17:00hr).....	34
Figure 6-3: Time series map of cloud affected water surface temperature	35
Figure 6-4: Surface temperature of water (K) (a) and net long wave radiation ($W m^{-2}$) (b) of the 16 th of September 2011 at 10:00hr local time	35
Figure 6-5: Diurnal cycle of incoming long wave (R _{li}) and outgoing long wave (R _{lo}) radiation (from 15 th of September 2011 at 18:00hr to 16 th of September 2011 at 17:00hr local time) combined with surface temperature(WST) for a pixel having ground measurement	36
Figure 6-6: Net radiation (Wm^{-2}) at 10:00 hour local time of the 16 th of September 2011	37

Figure 6-7: Diurnal cycle of net radiation (from 15 th of September 2011 at 18:00hr to 16 th of September 2011 at 17:00hr)	37
Figure 6-8: latent heat flux at 10:00hr local time of the 16 th of September 2011	38
Figure 6-9: Hourly at 10:00hr local time and daily evaporation 16 th of September 2011 (a and b respectively)	39
Figure 6-10: Time series map showing the hourly estimate of evaporation	39
Figure 6-11: Diurnal cycle of evaporation.....	40
Figure 6-12: Remote sensing and In situ measurement of net radiation ($W m^{-2}$).....	41
Figure 6-13: Diurnal cycle of evaporation from in situ measurement and remote sensing	42

LIST OF TABLES

Table 3-1: Data collected and instrument used (Date: - 09/15/2011 -09/16/2011)	10
Table 3-2: Data collected and instrument used (Date: - 09/17/2011 -09/18/2011)	10
Table 3-3: Data collected and instrument used (Date: - 09/21/2011 -09/22/2011)	11
Table 3-4: Spectral channel characteristic of the MSG/SEVIRI (Maathuis et al., 2011).....	12
Table 4-1: Coefficients for four channel algorithm(Sun and Pinker, 2007).....	22
Table 5-1: Daily estimate of evaporation (Date: 15/09/2011, 18:00hr-16/09/2011, 17:00hr)	32
Table 5-2: Daily average of the component of energy balance	32
Table 6-1: Parameters affecting the estimate of evaporation	40
Table 6-2: Comparison of average daily flux (all values in $W m^{-2}$)	42
Table 6-3: Comparison of methods and conditions of measurement	43
Table 6-4: The estimated daily evaporation.....	43
Table 6-5: Comparison with previous study of Alebachew (2009) (all values in $W m^{-2}$) for 11:00hr local time	43

1. INTRODUCTION

1.1. Background

Lakes and reservoirs are landscape features with great significance for people in social, cultural and economic aspects in everyday life. Lakes and reservoirs give water for irrigation, hydroelectricity, fishing, recreation, transport and the like. Therefore the study of the water budget of these systems is crucial. From the components of the water budget lake evaporation comprises a significant portion which is considered as a loss term in the lake water balance.

Water is a renewable resource and its economic value is recognized after the shortage of water comes true in different parts of our planet earth. This shortage leads to the establishment of an understanding of its great economic value as a natural resource. As part of the planet earth, this issue is facing in the Lake Tana and its surrounding and it needs proper water resource management. For the proper management and utilization of this resource there should be good understanding of the water balance of the Lake Tana. Accurate estimate of evaporation in the lake area would allow accurate calculation of water use by the different sectors of beneficiaries. This in turn will allow more effective use of available water resources. Also, accurate estimation of losses enables the policy and strategy makers to device the way to reduce these losses.

The process of evaporation is mostly controlled by the supply of energy required for the phase change from liquid water to water vapour, the supply of water and the transport mechanism which carries the water vapour away from the surface. The supply of energy, which is directly from the sun, is influenced by inclination angle, the cloudiness and the sunshine hours. For open water evaporation the availability of water is not a problem. The transport mechanism is greatly affected by the wind speed. Also Granger et al (2011) showed the hourly rate of open water evaporation is most strongly affected by the wind speed over the lake.

Since evaporation is a major component of the water budget its estimation of the hourly rate of evaporation in turn is of great importance. From the diurnal cycle of evaporation we can understand which parameter (wind speed, temperature and net radiation) is affecting the process of evaporation most.

1.2. Problem definition

Evaporation is one of the major components of the hydrologic cycle and is most difficult to estimate accurately. The estimation of evaporation from open water is difficult in that the necessary meteorological parameters are rarely measured over the water surface and the land based measurements are rendered by the thermal lag between the land and the water surface. The land based meteorological data for estimating evaporation over the lake also lacks to represent the surface characteristics of the lake water. For estimation of open water body evaporation the meteorological variables should be measured at the water surface.

For better understanding of the open water evaporation of Lake Tana it is important to understand its diurnal cycle. To better understand the diurnal cycle, representative in situ data need to be available directly from the surface of the water that need to be combined with the remote sensing data for its

spatial and temporal coverage over the lake. This would allow for the estimation of all energy balance terms that affect the evaporation rate.

1.3. Objective(s) and research questions

The main objective is to estimate the diurnal cycle of open water evaporation of the Lake Tana using ground measurement data and remote sensing. Remote sensing is used because of the lack of meteorological data over the water surface and since it provides data in a spatially and temporally coherent manner.

Specific objectives: -

- To estimate the water heat flux.
- To estimate the sensible heat flux.
- To estimate the net radiation.
- To estimate the latent heat flux.
- To retrieve surface temperature of the lake using remote sensing.

Research questions: -

- How large is the water heat flux?
- How is the variability of the Bowen ratio throughout the day?
- How well does the evaporation estimate at the pixel level much to the measured evaporation at the lake?

1.4. Previous studies

Previous studies have been conducted for the estimation of evaporation. There are studies which are undertaken to estimate open water evaporation from the Lake Tana water bodies, but due to the lack of previously taken data and well established meteorological stations their output result are not reliable. The study conducted by Kebede (2006) used the Penman open water approach to estimate the evaporation but the data they took for shortwave radiation calculation is from Addis Ababa (565km away from the lake) which doesn't represent correctly the lake area. In addition to these the studies were based on meteorological data from the land surface meteorological stations. Recently a study is also conducted by Alebachew (2009) who collected different meteorological data on the lake surface by traveling with the boat for the estimation of open water evaporation and Berhanu (2010) who also collected the data in a similar way and modeled the annual heat storage change of the lake Tana. But both of them didn't acquire the meteorological data from a single point on the lake surface, since they are travelling at the lake surface while collecting the data.

1.5. Thesis outline

Chapter two describes the literature review and discusses the theoretical background of the open water evaporation and the application of remote sensing.

Chapter three describes the study area and the input data collection for the application of the open water evaporation methodology. The fourth chapter explains the methodology applied for the estimation of open water evaporation. The fifth chapter discusses the in situ data analysis and the discussion of the result obtained. The sixth chapter aims at the estimation of open water evaporation using the techniques of remote sensing and the discussion of the results found.

Lastly, in the seventh chapter, the conclusion and recommendation are presented.

2. LITERATURE REVIEW

2.1. The process of evaporation

The process of evaporation involves a state change from liquid to vapour, which is fundamentally a physical phenomenon. However, in the natural world, evaporation from the land surface to the atmosphere generally occurs from complex interface that comprises plants, soils and air, and within this interface evaporation can arise both from within and from the surface of the plants and soil with respect to the meteorological conditions.

Land surface evaporation includes evaporation from the soil and plant transpiration. Open water evaporation is rather different from the land surface evaporation. Open water evaporation is mainly influenced by the supply of energy to provide the latent heat of vaporization and the ability to transport the vapour away from the surface of the water. In this process the availability of water does not limit the process, since it is always available. The energy source is the solar radiation and the ability to transport vapour away from the surface of the water depends largely on the wind velocity and the specific humidity.

The incoming solar radiation is the major source of energy for evaporation. For land surfaces the solar radiation is converted to sensible and latent heat at the soil or vegetation surfaces. In contrast, at the surface of the water the solar radiation is not all absorbed. Part of it may penetrate to great depths in clear water. In the study undertaken in Lake Elephant Butte, USA (Eichinger et al., 2003) the solar energy is observed to penetrate up to 30m of water depth and stored in the water .

The depth of solar radiation penetration differs with wave length and the composition of the water. The composition of the water affects the depth of penetration in that the water may contain sediments, salts, algae and etc. Solar radiation absorbed below the water surface is stored as energy and is not immediately used for evaporation or for sensible heat. The energy stored results in a lag of evaporation compared to the solar radiation, and there is less total annual evaporation than when there is no substantial energy storage. For shallow water bodies, like Lake Tana, the amount of energy stored may not be large, but affects largely the daily evaporation rates.

2.2. The estimation of open water evaporation

Because of its nature, evaporation from open water bodies, like lakes, is rarely measured directly. Evaporation from open water bodies is most commonly computed indirectly by one or more methods. Dingman (2002) explains the methods for open water evaporation estimation. These are the Water-balance approach, Mass-transfer approach, Eddy- correlation approach, Energy-balance approach, Penman or combination approach and Pan-evaporation approach.

The selection of the method for a particular computation is largely determined by the availability data, size of the water body, and the desired accuracy. Also the method to be selected depends on the type of evaporative surface, the stored energy use and the water advected energy use.

2.3. Diurnal cycle of evaporation

Evaporation from natural lands surfaces often shows a high variation during the period of a day, mostly in response to the daily variation of the radiant energy input at the surface. This makes it difficult to estimate the total daily evaporation when only one or a few instantaneous estimates of evaporation are available. It

is often possible to tackle this difficulty by assuming the relative partition of energy flux among its components is the same in the diurnal cycle of the surface energy balance. Therefore, if the relative partition of total incoming energy flux among the different components is the same, the ratio of latent heat flux to any other flux component can be taken as constant through the day. This concept of constant flux ratios is tested by Brutsaert and Sugita (1992).

Evaporation from open water bodies is the main component of the energy and hydrologic cycles for many watersheds. Since most hydrological and meteorological models work with time steps of the order of an hour, a reliable approach to the calculation of hourly lake evaporation is essential. However, evaporation from open water remains largely unmeasured as a course of routine and is still estimated with limited confidence. This is mainly true for sub-daily time periods, where the factors leading the boundary layer dynamics, the thermal lag between the water and land surfaces, and the evaporation rates are not well understood.

2.4. The application of remote sensing

Remote sensing techniques are used throughout the world to measure a very diverse set of environmental features, like the wave heights, bathymetry, topography, water quality, land cover and surface temperature. It is a powerful tool in acquiring the required data for open water body evaporation. It has the ability to capture the required meteorological data at the required temporal resolution and spatial coverage. Due to this it provides representative data of several hydrological parameters from point measurement to a large scale as required. Therefore in order to use these remotely sensed data there is a need of an algorithm. For this effect there are many surface energy balance system (SEBS) algorithm developed by different researchers e.g. (Bastiaanssen, Menenti, et al., 1998; Bastiaanssen, Pelgrum, et al., 1998; Su, 2002) and others. The energy balance approach considers the supply of energy for vaporization in the evaporation process for the change of state of water. There is also the aerodynamic approach in which wind is an important factor in transporting the water vapour away from the evaporating surface.

Compared to in situ methods, advantages of remote sensing include the capacity to instantaneously acquire large areas of the Earth's surface. A relatively time consuming and the potentially costly in situ data collection can be minimized with remote sensing.

3. STUDY AREA AND DATA COLLECTION

3.1. Study area

Lake Tana is located in the North-western highlands of Ethiopia at 12°00' N and 37°15' E. The lake has an altitude of 1786m.a.s.l. with a surface area of 3000 km², comprising about 20% of the 15000km² drainage area. The lake is fed by seven permanent and 40 seasonal rivers. The main tributaries to the lake are Gilgal Abbay from the south, Gumara and Rib from the east and Megetch river from the north and only small river system drains from the western side (Rientjes et al., 2011) and the Lake Tana basin is shown in figure 3-3. Wale (2008) indicates that the contribution from ungauged catchment is about 42% of the total annual inflow. The only outflow from the river is the Blue Nile. Lake Tana, having an average depth of 8m and maximum depth of 14m (Wale, 2008) (see also figure 3-2), is the largest lake in Ethiopia and the third largest in the Blue Nile basin.

The lake has been formed by volcanic activity, blocking the course of inflowing rivers in the early Pleistocene time 5 million years ago. The lava also separated the lake and its headwaters from the Blue Nile basin by 40m high falls at Tissisat, 30km downstream of the lake. Starting from 2001 the lake is also functioning as a reservoir for Tis_abbay-2 Hydroelectric project which is generating 78 MW of electricity.

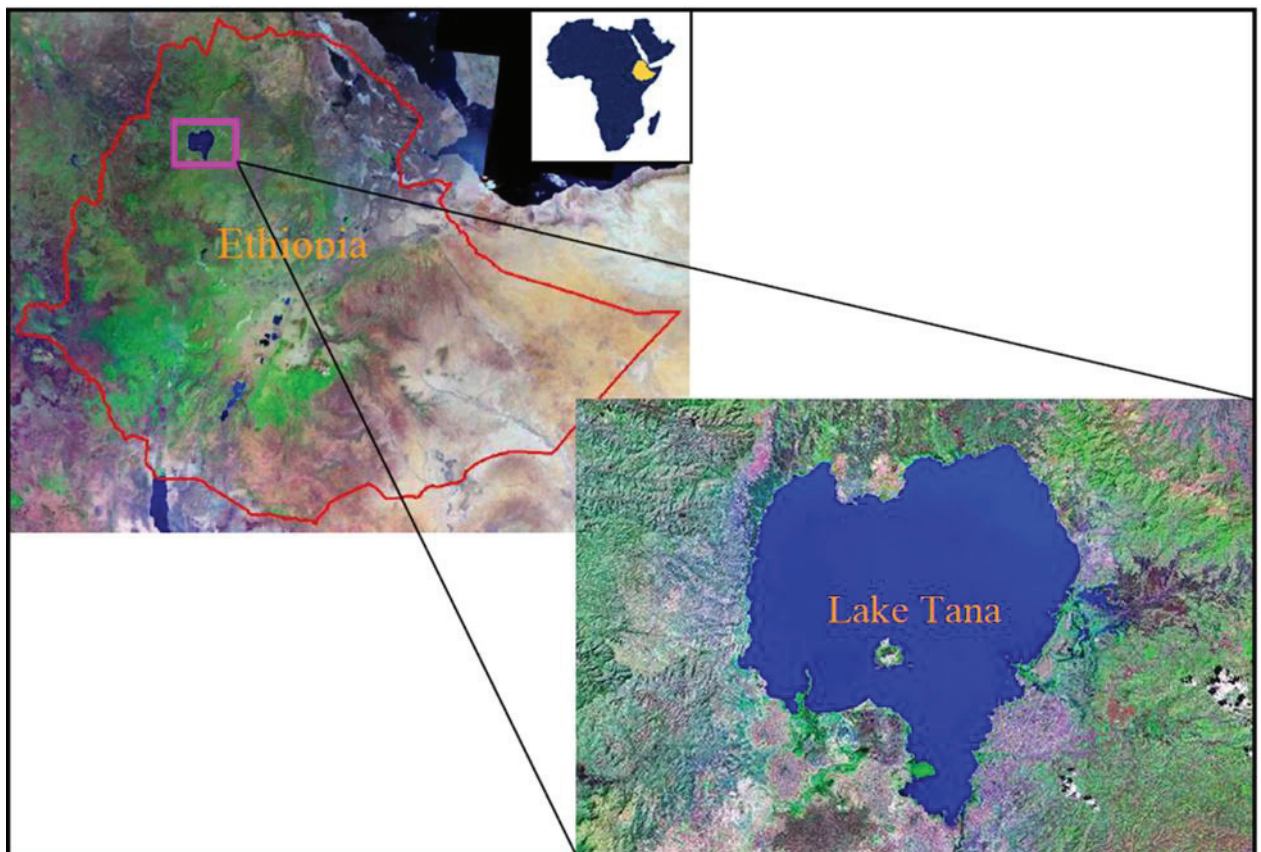


Figure 3-1: Location of the study area, Lake Tana (false colour composite of LANDSAT7 image, October 2003)(Abreham Kibret, 2009)

The climate of Lake Tana area is typical of semi-arid regions near to the Equator, with a high diurnal temperature variation between day times maximum of 30°C to night minimum of 6°C. The rainfall is up to 2000 mm per year in a rainy season from May to October. The inflow to the lake is $10.3 \times 10^9 \text{ m}^3 \text{ yr}^{-1}$ and the outflow is $3.7 \times 10^9 \text{ m}^3 \text{ yr}^{-1}$, which is 36% of the inflow. This difference of inflow and outflow is caused by the high evaporation losses and the water residence time which is 3 years. During October to June evaporation exceeds input through rainfall and during this time many of the inflowing streams dry up totally (Vijverberg et al., 2009). Wind speeds shows a marked diurnal pattern, during the night and morning wind speed is generally below 1.5 m s^{-1} , but in the afternoon starting at noon and going on until the evening wind speeds are generally between 3.0 and 4.8 m s^{-1} (Vijverberg et al., 2009).

Lake Tana has a large storage capacity that only responds slowly to the various processes of the climatic and hydrological cycles. Annual lake level fluctuations are approximately 1.6m. The lake has historic maximum and minimum water levels of 1788.02m at the 21st of September 1998 and 1784.46m at the 30th of June 2003 (Rientjes et al., 2011).

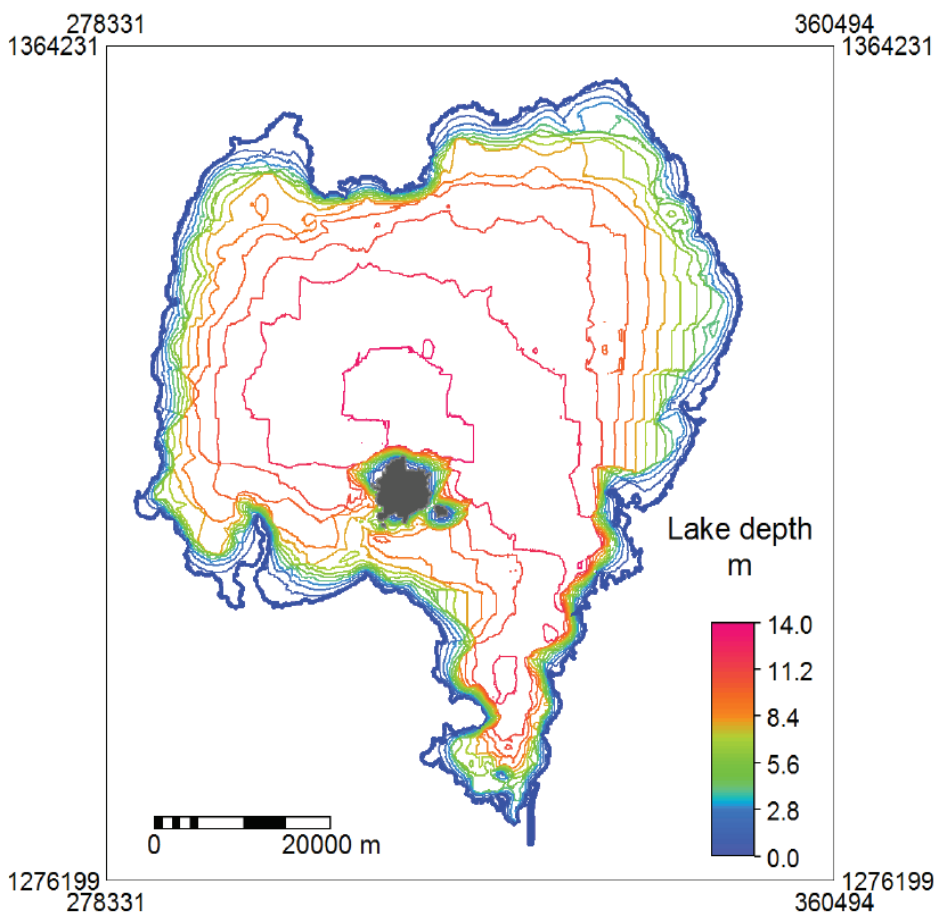


Figure 3-2: Depths of Lake Tana (Wale, 2008)

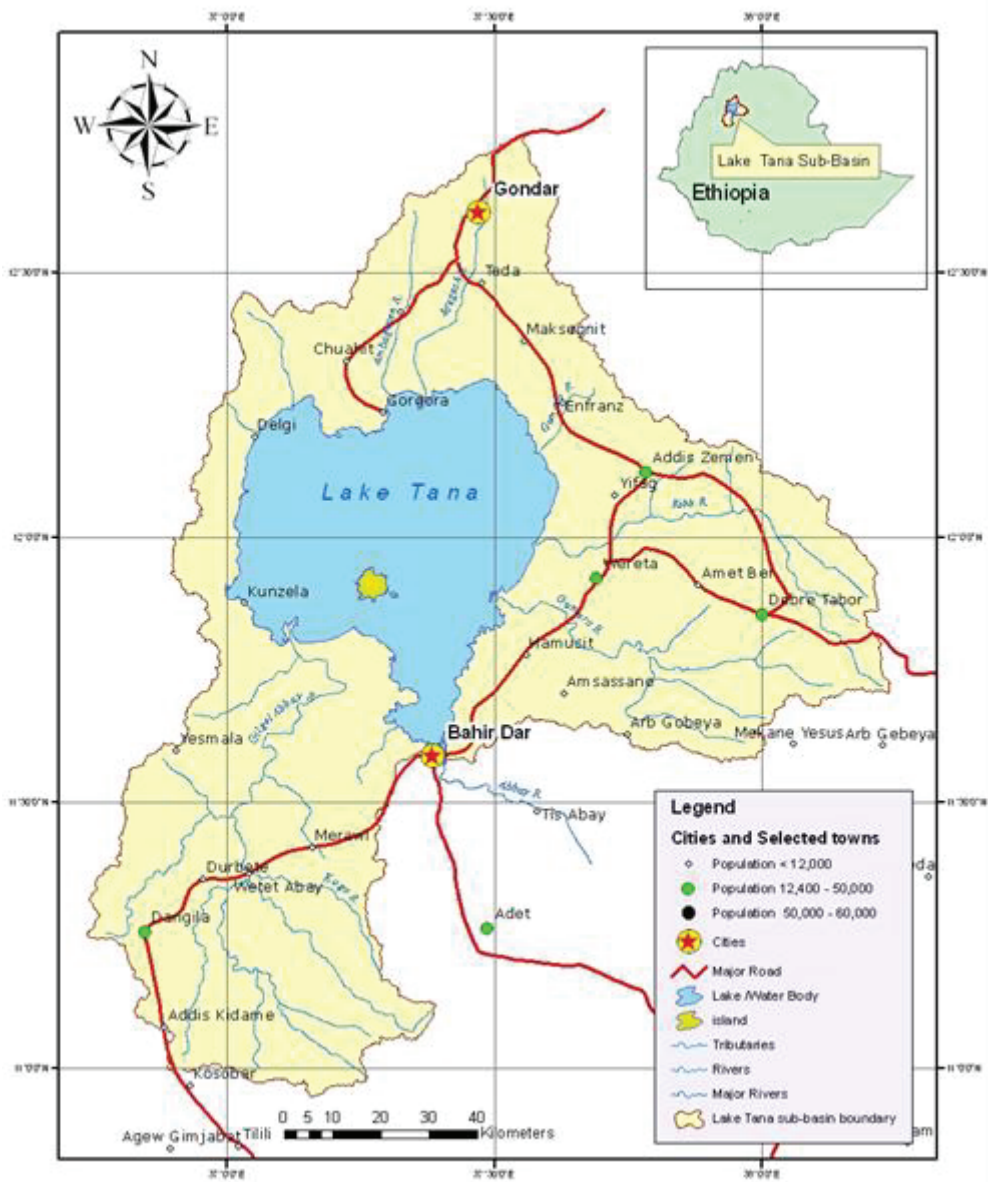


Figure 3-3: Lake Tana basin (source: Ethiopian ministry of water recourses).

3.2. In situ data collection

To gather in situ data for this research work a field work is undertaken starting from the 7th of September 2011 to the 2nd of October 2011. This field campaign served to collect a 24 hours continuous data from the Lake Tana. Data are collected at the lake surface for a single location. The data collected are the temperature profile at different depths in the water and air, wind speed, relative humidity, water surface temperature, incoming short wave radiation and the respective GPS reading for the measurement location (i.e. point).

For the collection of data the instruments are installed in a special float constructed at the site. The construction of the float is such that effects of a wave of water were not to disturb the required height and depth of the instrument and sensors above and below the water surface. Also the float is free to move up and down with respect to the water surface (see Figure 3-4 and 3-5).



Figure 3-4: setting up of instruments on the Lake Tana

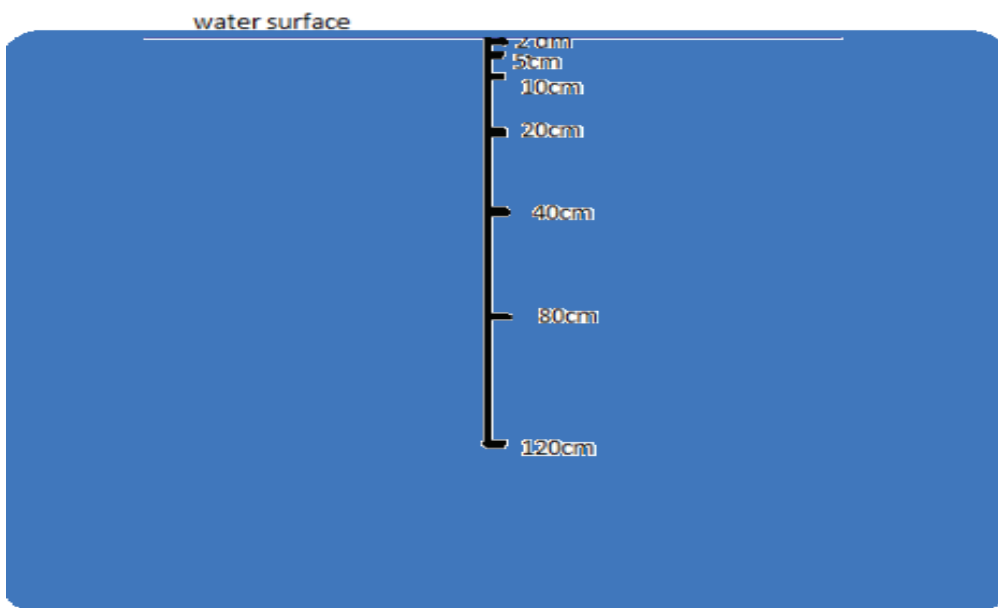


Figure 3-5: setting up of temperature sensors below the Lake surface

The anemometer, Pyranometer and the Temperature-Humidity probe are mounted at height of 2m above the water surface on the float. The temperature sensors are fixed on a wooden pole at a depth of 120, 80, 40, 10, 5 and 2cms below the water surface and 2 and 200cms above the water surface.

For recording the data two type of loggers are used. A CR-200 Campbell-Scientific (see figure 3-6) is used for recording the data from the anemometer, Pyranometer and the Temperature-Humidity probe and two HOBO 4- channel external data loggers were also used for recording the eight temperature sensors. The CR-200 Campbell-Scientific is programmed with the software Loggernet to record the data at a time interval of five minute and the HOBO-loggers are programmed by the use of BoxCar Pro to record the same time interval.

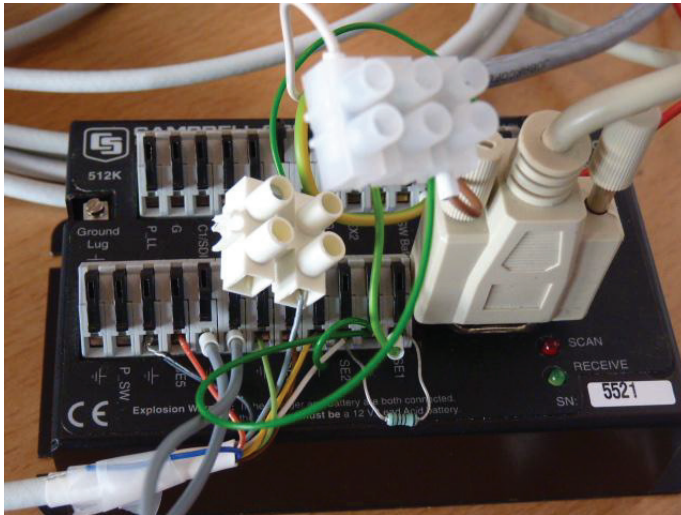


Figure 3-6: The CR-200 Campbell-Scientific data logger, the HOBO 4-channel external data logger and the Thermometer Infrared Testo 830-T2

The Infrared gun surface temperature record (Thermometer Infrared Testo 830-T2) (see figure 3-6) and the GPS location ($11^{\circ}37'28.78''\text{N}$ and $37^{\circ}21'32.94''\text{E}$) is taken manually. The infrared surface temperature measurement is taken at 5 minute interval for the first hour to observe the rate of change of temperature and for the remaining time period it is made at 30 minute interval. The Thermometer Infrared Testo 830-T2 also measures the emissivity of the water surface. The equipment's which were used and their respective time period and type of measurement are presented in Table 3-1, 3-2 and 3-3.

Measurements were taken for three 24 hours cycles with in the field campaign period. The first day field work starts on the 15th of September 2011 at 16:40 hour and ends on 16th of September 2011 at 17:20 hour's local time. All the intended measurements are taken even though the sky is covered by cloud and it is raining in some hours of the day and night.

The second day field work starts from the 17th of September 2011 at 16:20 hour and ends at 18th of September 2011 at 17:00 hours. The second day measurement is not complete and has incorrect data due to failure of the batteries that were used for the anemometer, Pyranometer and the temperature-humidity probe. The temperature sensors, which uses an independent battery source and logger, has recorded properly and also the infrared surface temperature measurement is made (see Table 3-2).

After replacing the batteries the third day measurement at the 19th of September 2011 was tried to make. But at this period the weather condition of the site is seriously bad, having a very high wind, rain and water wave, and overturned the whole set of the instrument into the lake. The data recorded in the loggers was downloaded to the PCs and checked for its consistency which revealed the wind and temperature-humidity probe (which has unreliable value compared with the first day measurement) are not working correctly.

A fourth day of measurement, which doesn't include the wind speed measurement, is undertaken starting from the 21st of September 2011 at 16:50 hour and ends at the 22nd of September 2011 at 17:25 hour. But at this time the infrared gun battery was empty and a compatible battery is not found in the local market therefore the surface temperature is not measured (see Table3-3).

Table 3-1: Data collected and instrument used (Date: - 09/15/2011 -09/16/2011)

No	Measurement	Instrument used	Length of measurement period	Remark
1	Wind_Avg	Anemometer	09/15/11,16:40- 09/16/11, 17:30	
2	Rad_Avg	Pyranometer	09/15/11,16:40- 09/16/11, 17:30	
3	T_Avg	Temp-humidity probe	09/15/11,16:40- 09/16/11, 17:30	
4	RH_Avg	Temp-humidity probe	09/15/11,16:40- 09/16/11, 17:30	
5	Temperature profile	Temperature sensors	09/15/11,16:40- 09/16/11, 17:30	
6	Surface temp of the water	Infrared gun	09/15/11,16:40- 09/16/11, 17:00	
7	Geographic location	GPS	One measurement	

Table 3-2: Data collected and instrument used (Date: - 09/17/2011 -09/18/2011)

No	Measurement	Instrument used	Length of measurement period	Remark
1	Wind_Avg	Anemometer	09/17/11, 16:40- 09/18/11, 04:55	Not measured
2	Rad_Avg	Pyranometer	09/17/11, 16:40- 09/18/11, 04:55	Not measured
3	T_Avg	Temp-humidity probe	09/17/11, 16:40- 09/18/11, 04:55	Not measured
4	RH_Avg	Temp-humidity probe	09/17/11, 16:40- 09/18/11, 04:55	Not measured
5	Temperature profile	Temperature sensors	09/17/11, 16:40- 09/18/11, 17:00	
6	Surface temp of the water	Infrared gun	09/17/11, 16:40- 09/18/11, 17:00	
7	Geographic location	GPS	One measurement	

Table 3-3: Data collected and instrument used (Date: - 09/21/2011 -09/22/2011)

No	measurement	Instrument used	Length of measurement Period	Remark
1	Wind_Avg	Anemometer	09/21/11, 16:50- 09/22/11,17:25	Not measured
2	Rad_Avg	Pyranometer	09/21/11, 16:50- 09/22/11,17:25	
3	T_Avg	Temp-humidity probe	09/21/11, 16:50- 09/22/11,17:25	
4	RH_Avg	Temp-humidity probe	09/21/11, 16:50- 09/22/11,17:25	
5	Temperature profile	Temperature sensors	09/21/11, 16:50- 09/22/11,17:25	
6	Surface temp of the water	Infrared gun	09/21/11, 17:00- 09/22/11,17:00	Not measured
7	Geographic location	GPS	One measurement	

3.3. Remote sensing data

Satellite imagery from the MODIS, MSG/SEVIRI and the LSA SAF products are used in this study.

3.3.1. MODIS

The Moderate resolution Imaging Spectroradiometer (MODIS) is an instrument on the Terra and Aqua satellite. Terra is found at an altitude of 705Km and has a cross track swath of 2330Km and along track swath of 10Km. Terra travels from north to south across the equator at 10:30 local time in the morning having a scan rate of 20.3 rpm (i.e. revolution per minute) and Aqua travels from south to north over the equator at 13:30hr local time in the afternoon. Terra MODIS and Aqua MODIS are viewing the entire Earth's surface every 1 to 2 days, acquiring data in 36 spectral bands, or groups of wavelengths and design life of 6 years (see MODIS Technical Specifications).

The MODIS data can be downloaded from the NASA website <http://modis-land.gsfc.nasa.gov/> and it is free of charge. The product gives both black-sky albedo and white-sky albedo.

3.3.2. The MSG/SEVIRI

The Meteosat Second Generation (MSG) is a geostationary satellite developed by the European Organization for the exploitation of Meteorological Satellites (EUMETSAT) in close co-operation with the European Space Agency (ESA). SEVIRI is one of the instruments on board of the MSG. The MSG/SEVIRI is a 50 cm-diameter aperture, line-by-line scanning radiometer, which provides image data in four Visible and Near-InfraRed (VNIR) channels and eight InfraRed (IR) channels. The main characteristic of SEVIRI is its continuous imaging of the Earth in 12 spectral channels with a repeating cycle of 15 min. The imaging sampling distance is 3 km at the sub-satellite point for standard channels, and down to 1 km for the High Resolution Visible (HRV) channel (Schmid, 2000). Channel spectral characteristics and the main area of uses of each channel are presented in Table 3-4.

Table 3-4: Spectral channel characteristic of the MSG/SEVIRI (Maathuis et al., 2011)

Channel	Spectral characteristics band (um)			Main observational application
	Centre	Min	Max	
VIS0.6	0.635	0.56	0.71	Surface, clouds, wind fields
VIS0.8	0.81	0.74	0.88	Surface, clouds, wind fields
NIR1.6	1.64	1.5	1.78	Surface, cloud phase
IR3.9	3.9	3.48	4.36	Surface, clouds, wind fields
WV6.2	6.25	5.35	7.15	Water Vapour, high level clouds, atmospheric instability
WV7.3	7.35	6.85	7.85	Water Vapour, atmospheric instability
IR8.7	8.7	8.3	9.1	Surface, clouds, atmospheric instability
IR9.7	9.66	9.38	9.94	Ozone
IR10.8	10.8	9.8	11.8	Surface, clouds, wind fields, atmospheric instability
IR12.0	12	11	13	Surface, clouds, atmospheric instability
IR13.4	13.4	12.4	14.4	Cirrus cloud height, atmospheric instability
HRV	Broad band (0.4-1.1)			Surface, clouds

The MSG/SEVIRI sensor provide data to EUMETSAT at Darmstadt (Germany) which is processed and uplinked to HOTBIRD-6 in wavelet compressed format (Gieske et al., 2005). The images are received and archived at ITC in compressed form and for academic and research purpose, the archive is accessed through the internal network.

The retrieval of MSG is done using the import utilities developed in UT-ITC. When using the MSG retrieval the executed commands can be saved as a text file and can be used to retrieve any other image required by editing the saved text file in the ILWIS software. Figure 4-2 shows the MSG Data Retriever window which is designed by Retsios et al (2006).

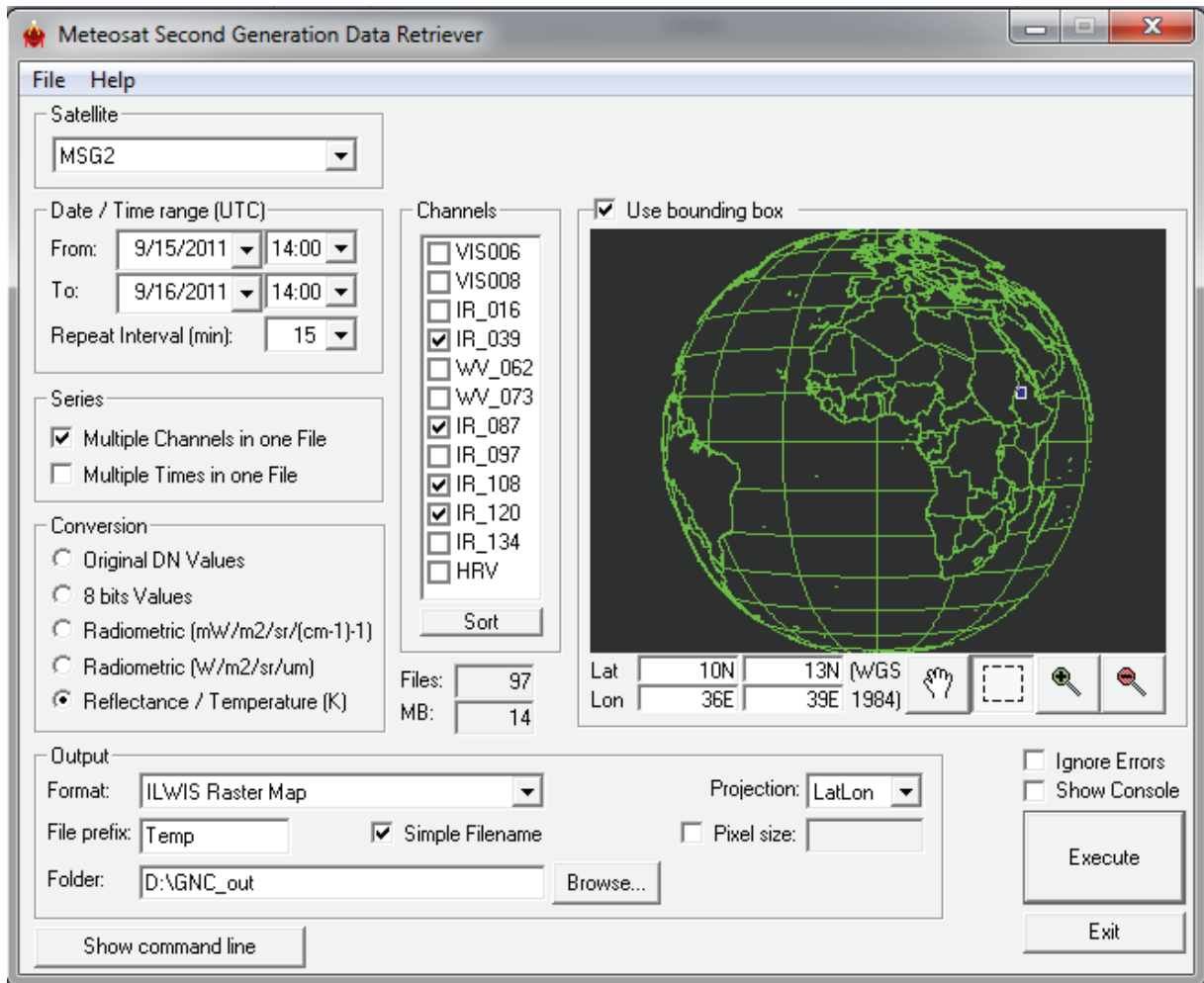


Figure 3-7: MSG Data Retriever Window as a plug-in in ILWIS GIS software version 1.3.

3.3.3. The Land Surface Analysis Satellite Application Facility (LSA SAF)

The main purpose of Land Surface Analysis Satellite Application Facility (LSA SAF) is to increase the benefit from the EUMETSAT satellite (MSG and EPS) data related to land, land-atmosphere interaction and biospheric application by generating, archiving and disseminating the products. The down welling short wave flux (DSSF) and down welling long wave flux (DSLW) are directly downloaded from LSA SAF web dissemination service site <http://landsaf.meteo.pt/> and it is also free of charge. The product has a temporal resolution of 30 minute and spatial resolution of 3km.

4. METHODOLOGY

4.1. Estimation of evaporation using in situ data

In this study four methods are used; the Energy balance, the Penman combination equation, the Bowen ratio and the Bowen ratio-Energy balance methods.

4.1.1. The Penman combination equation

Howard Penman derived an equation in 1948 to estimate the evaporation from the open water surface by combining the vertical transfer of sensible heat and water vapour with surface energy balance equation. This method is further developed and modified by Maidment (1993) and it reads:-

$$E = \frac{\Delta}{\Delta + \gamma} (R_n - G) + \frac{\gamma}{\Delta + \gamma} \frac{6.43(1 + 0.536U_2)D}{\lambda} \quad (4-1)$$

Where:

E	=the evaporation that occurs from free water surface	[mmday ⁻¹]
Δ	=the slope of saturated vapour pressure curve	[-]
R_n	=the radiation exchange of the free water surface	[mm day ⁻¹]
G	=the water heat flux	[mm day ⁻¹]
U_2	=the wind speed measured at 2 m	[ms ⁻¹]
D	=the average vapour pressure deficit	[kPa]
λ	= the latent heat of vaporization	[MJkg ⁻¹]
γ	=psychometric constant	[kPa°C ⁻¹]

The vapour pressure deficit (D) is the difference between the amount of moisture in the air and how much moisture the air can hold when it is saturated. It is expressed mathematically as: -

$$D = e_s - e_a \quad (4-2)$$

Where:

e_s	= the saturated vapour pressure	[mbar]
e_a	= the actual vapour pressure	[mbar]

The slope of the saturated vapour pressure curve (Δ) reads:

$$\Delta = 4098 \frac{e_s}{((T_a - 273.16) + 237.3)^2} \quad (4-3)$$

The psychometric constant (γ) reads:

$$\gamma = 1630 \frac{P}{\lambda} \quad (4-4)$$

Where: P is the air pressure [mbar] of air.

4.1.2. The energy balance method

The energy balance method is considered as an advanced method for the estimation of the evaporation and reads

$$\lambda E = R_n - G - H \quad (4-5)$$

Where: H is the sensible heat flux [wm^{-2}], λE the latent heat flux (λ the latent heat of vaporization in Jkg^{-1} , and E the evaporation rate in $\text{Kg s}^{-1}\text{m}^{-2}$).

- **Water heat flux**

This is the energy used for heating of the water. It is positive when water is warming and negative when water is cooling. It is important to investigate the hourly heat storage change which is evaluated from the temperature profile with respect to time and depth.

$$G(0) = \rho c_p \int_{z=0}^{\infty} \frac{\partial T}{\partial t} dz' \approx \rho c_p \sum_{i=1}^n \frac{\Delta T}{\Delta t} \Delta z_i \quad (4-6)$$

Where:

ρ = the density of water [Kg m^{-3}]

c_p = the specific heat capacity of water [JKg $^{-1}$]

$\frac{\Delta T}{\Delta t}$ = the change in temperature with two consecutive measurements [Ks $^{-1}$]

Z = is the depth below the surface [m]

Δz_i = thickness of a water layer between two measurements points [m]

n = the number of temperature measurements in the profile. The deepest should be sufficiently deep such that it is not affected by the diurnal cycle of temperature.

- **Net radiation**

In the absence of restriction due to shortage of water at the evaporative surface, the amount of radiant energy captured at the earth's surface is the major factor in controlling evaporation. The importance of this parameter is that it is the major portion of energy available at the earth's surface to drive the process of evaporation and water heat flux.

The net radiation is the difference between the net short wave and net long wave radiation.

$$R_n = R_s \downarrow - R_s \uparrow + R_l \downarrow - R_l \uparrow \quad (4-7)$$

Where: $R_s \downarrow$ and $R_s \uparrow$ are the incoming and outgoing short wave radiations and $R_l \downarrow$ and $R_l \uparrow$ are the incoming and outgoing long wave radiations (both terms in Wm^{-2})

- **Net long wave radiation**

The rate of the outgoing long wave radiation is proportional to the temperature of the surface raised to the fourth power. This relation is expressed quantitatively by the Stefan-Boltzmann law. The net long wave radiation leaving the earth's surface is less than that emitted by the earth's surface. Since cloud and humidity are the major factor, the Stefan-Boltzmann law is corrected by these two factors when estimating the net outgoing long wave radiation. The net Long wave radiation is the difference between the emission from the earth surface and the radiation from the atmosphere. The net long wave radiation is calculated using the Stefan Boltzmann's equations (Brutsaert, 2005).

I. Long wave incoming

The down ward long wave radiation can be calculated accurately on the basis of vertical profile data of humidity and temperature. Such data are not always available; as a result simpler method can be used that depends on the available data of air temperature and humidity near the ground.

$$R_l \downarrow = \varepsilon_a \sigma T_a^4 \quad (4-8)$$

Where: ε_a is the atmospheric emissivity of air, σ is the stefan boltzman constant ($=5.6697 \times 10^{-8} \text{ w m}^{-2} \text{ k}^{-4}$) and T_a is the temperature of the air in [k].

II. Long wave outgoing

The outgoing long wave radiation is usually calculated by assuming that the water surface under consideration is equivalent with an infinitely deep gray body of uniform temperature and emissivity which is close to unity.

$$R_l \uparrow = \varepsilon_s \sigma T_s^4 + (1 - \varepsilon_a) R_l \downarrow \quad (4-9)$$

Where: ε_s the emissivity of the water and T_s is the temperature of the water surface in [k].

- **Net short wave radiation**

The dominant energy component driving the earth's climate process and energy balance is the short wave radiation emanating from the sun. Shortwave radiation is the radiant energy emitted by the sun in the visible and near-ultraviolet wavelengths (between about 0.1 and 2 micrometers).

$$R_s \uparrow = \alpha R_s \downarrow \quad (4-10)$$

Where: $R_s \uparrow$ is the outgoing short wave radiation, $R_s \downarrow$ is the incoming short wave radiation and α is the surface albedo.

The surface albedo is the ratio of the short wave reflected radiative flux and the flux of the corresponding incident radiation. The outgoing short wave radiation is calculated using the Albedo (α) of the water surface. Alebachew (2009) suggested an albedo value of 0.1 for Lake Tana for the month of September and is adapted here to estimate the outgoing short wave radiation.

- **Sensible heat flux**

The sensible heat flux is a phenomenon that allows the earth to exchange heat between the body of water and the atmosphere when there is a temperature difference between them. The sensible heat flux reads:

$$H = \frac{\rho_a c_p}{r_{ah}} (T_s - T_a) \quad (4-11)$$

Where: ρ_a is air density [Kg m^{-3}], c_p specific heat of moist air, $1004 \text{ J Kg}^{-1} \text{ K}^{-1}$, r_{ah} is the aerodynamic resistance to heat transport [s m^{-1}], T_s is the water surface temperature [K], and T_a is the air temperature [K] at measuring height.

The aerodynamic resistance to heat transport (r_{ah}) is calculated from: -

$$r_{ah} = \frac{1}{K^2 U} \left[\ln \left(\frac{Z}{Z_0} \right) \right]^2 \quad (4-12)$$

Where: K is the Van Karman's constant [taken 0.41], U is the wind speed at 2m [m s^{-1}], Z is the measurement height [m] and Z_0 is the roughness height of the wave [m].

The measurement height (Z) is 2m and the roughness height of the wave (Z_0) is taken as 0.00137m as given by Penman for open water surface and is adopted for this research.

4.1.3. The Bowen ratio/Energy balance (BREB) method

The Bowen ratio/Energy balance (BREB) is a micrometeorological method often used to estimate latent heat flux because of its simplicity, robustness, and cost (Todd et al., 2000). This method is the combination of the energy balance and the Bowen ratio method. In the Bowen ratio/ energy balance method (BREB), the evaporation is calculated as:-

$$E = \frac{R_n - G}{\lambda(1 + \beta)} \quad (4-13)$$

The Bowen ratio (β) is the ratio of the sensible heat flux to the latent heat flux and is expressed as:

$$\beta = \frac{H}{\lambda E} = \gamma \frac{T_2 - T_1}{e_2 - e_1} \quad (4-14)$$

Where T_1 and e_1 are air temperature [K] and vapour pressure [m] at the measurement height z_1 and T_2 and e_2 are air temperature at measurement height z_2 , γ is the psychometric constant [mbar.K^{-1}].

4.1.4. The Bowen ratio method

The Bowen ratio method is one of the methods used to estimate the Latent heat flux (λE) and it only needs the estimate of the sensible heat flux (H) and the Bowen ratio (β). The Bowen ratio (β) is determined using the profile measurement of temperature and Vapour pressure. In this study the Bowen ratio is calculated for the whole day using in situ measurements of air temperature, surface temperature and vapour pressure.

The Latent heat flux can also be estimated using the Bowen ratio method which reads:

$$\lambda E = \frac{H}{\beta} \quad (4-15)$$

The difference of this method with the BREB method is that now H calculated with Eq.4-11 is used instead of the R_n-G calculated with Eq.4-7 and 4-6.

4.2. Estimate of evaporation using Remote sensing

4.2.1. Water heat flux

The water heat flux can be determined from the change in temperature profile with respect to time. The water heat flux for the open water can be estimate from the surface temperature of the water which is retrieved from the remote sensing data. Murray and Verhoef (2007) has shown the soil heat flux can be estimated from the surface temperature retrieved from the remote sensing. Using the same concept and methodology the water heat flux can also be estimated from the surface temperature of the water. However there are differences between water and soil heat flow:

- Thermal properties of water are different from soil.
- The water is mixed by the turbulent movement.
- There is transmittance and penetration and radiation in water, but not on the soil.

Due to the lack of cloud free data and time constraint change in temperature profile from the field measurement over the time is used instead of developing a method based on the remote sensing data of surface temperature.

4.2.2. Net radiation

The net radiation consists of the algebraic sum of the incoming and outgoing radiation flux components.

- **Net long wave radiation**

The net Long wave radiation is the difference between the emission from the earth surface and the radiation from the atmosphere.

$$R_{nl} = R_l \downarrow - R_l \uparrow \quad (4-16)$$

Incoming long wave radiation can be calculated according to the air temperature

$$R_l \downarrow = \varepsilon_a \sigma T_a^4 \quad (4-17)$$

Where, σ is the Stephan Boltzmann constant, taken $5.67 \times 10^{-8} \text{ Wm}^{-2} \text{ K}^{-4}$ as a default value, and ε_a is the emissivity of air described, T_a is the air temperature at the reference height.

The outgoing long wave radiation is determined as a function of surface temperature and emissivity as:

$$R_l \uparrow = \varepsilon_s \sigma T_s^4 + (1 - \varepsilon_s) R_l \downarrow \quad (4-18)$$

Where, ε_s and T_s are surface emissivity and temperature respectively. The emissivity can be calculated from the formula given by (Liang, 2004)

$$\varepsilon = 0.261 + 0.314\varepsilon_{31} + 0.411\varepsilon_{32} \quad (4-19)$$

ϵ_{31} and ϵ_{32} are the emissivity from channel 31 and 32 of the MODIS band.

- **Net short wave radiation**

The dominant energy component driving the earth's climate process and energy balance is the short wave radiation emanating from the sun. The net short wave radiation can be calculated from the equation given by Xue and Cracknell (1995) which reads:

$$R_s = (1 - \alpha) S_o C_t \cos \theta \quad (4-20)$$

Where α is the surface albedo, S_o is the solar constant (1367 Wm^{-2}), C_t is the atmospheric transmittance in the visible spectrum (typically 0.75), $\cos \theta$ is the solar zenith angle [-].

The net short wave radiation can also be calculated from the relation

$$R_{ns} = R_s \downarrow - R_s \uparrow \quad (4-21)$$

And the short wave outgoing can be derived from the relation

$$R_s \uparrow = \alpha R_s \downarrow \quad (4-22)$$

Since the albedo product of the MODIS is both for black sky albedo (BSA) and white sky the albedo (WSA) can be computed from the relation given by Roman et al (2009):

$$\alpha = (1 - DF)x(BSA_S_w) + (WSA_S_w) \quad (4-23)$$

Where α is the Total albedo, BSA_S_w is the black sky albedo from the short wave bands, WSA_S_w is the white sky albedo from the short wave bands and DF is the fraction of diffused sky light [=0.75].

4.2.3. Latent and Sensible heat flux

The latent heat flux can be determined from the relation

$$\lambda E = \frac{R_n - G}{(1 + \beta)} \quad (4-24)$$

Since it was not possible to develop a method for the estimation of the water heat flux and the Bowen ratio from the remote sensing data, the estimate made from the in situ data are used for the estimation of the latent heat flux instead of the remote sensing measurement.

The sensible heat flux is determined from the energy balance equation as

$$H = R_n - \lambda E - G \quad (4-25)$$

4.3. Surface temperature retrieval

The land surface temperature diurnal (LSTD) cycle is a significant climate parameter since it controls the upward terrestrial radiation and energy exchange between the earth surface and the atmosphere (Sun and Pinker, 2007). By studying the diurnal variation of the soil surface temperature Kimura and Shimizu (1994)

shows it is possible to estimate the values of the sensible and latent heat fluxes from the soil surface temperature and several commonly observed meteorological variables. Water temperature also plays a role in ecological functioning and in controlling the biogeochemical process of water body (Alcântara et al., 2010). Water surface temperature is an important parameter in the energy balance of the earth surface, and for this reason it is important for the study of energy exchange of the open water surface. Moreover, the difference in temperature of the water surface and the air controls the exchange of heat in the air and water boundary layer and this implies its importance to the understanding of the hydrologic cycle. The study of the water surface temperature using the common technique of ground measurement is expensive and time consuming and further if the water body that will be studied is large then problem will also be large like sampling problems. Remote sensing has the advantage to overcome the above mentioned problem and also the capacity to observe areas which are inaccessible by land.

Studies have been undertaken for the retrieval of land surface temperature (LST) using different satellites. But most of them focus, for their high spatial resolution of 1km, on polar orbiting satellites like the National Oceanic and Atmospheric Administration Advanced Very High-Resolution Radiometer (NOAA-AVHRR) (Becker and Li, 1990; Coll et al., 1994; Price, 1983) and the Moderate Resolution Imaging Spectroradiometer (MODIS) (Liang, 2001b). LST exhibits strong diurnal variation which cannot be captured by a polar orbiting satellite which observes a single location around twice per day. Due to its high variability in time and space and polar orbiting satellites are not able to capture this variability at a required time scale.

MSG satellite has the advantage of providing diurnal coverage with a higher temporal resolution compared with polar orbital satellites. Observations from the Spinning Enhanced Visible and Infrared Imager (SEVIRI) on the MSG satellite are available at 15-min intervals at a resolution of 3 km in four relevant channels. These features make the MSG/SEVIRI very attractive and in this study it is selected for water surface temperature retrieval.

4.3.1. Methods for retrieving LST

The estimate of surface temperature is derived from the radiance in thermal infrared spectrum. The remote sensing measured radiance at the sensor is partly from radiation emitted by the earth and partly from the atmosphere (and some of the radiation emitted by the earth is absorbed by the atmosphere). The atmospheric interference should be corrected and this can be done in two categories as discussed in AHAS (AVHRR Hydrological Analysis System) by Parodi (2002). The first is the direct methods which use radiation transfer models together with atmospheric radio sounding, satellite vertical sounder, and climatologically data. The second is the indirect methods are based on split-window or in situ temperature observations. From the available methods in this study the four channel algorithm is selected.

❖ The four channel algorithm

Sun and Pinker (2007) developed four-channel surface temperature (ST) algorithm based on the characteristics of the MSG/SEVIRI three-window thermal channels (8.7, 10.8, 12.0 μm) and one middle-infrared (MIR) channel (3.9 μm) and radiative transfer model simulations. The developed algorithm shows improvements in the determination of surface temperature. The middle infrared (3.9 μm) channel has low atmospheric absorption and attenuation, for this reason it is aimed to improve the atmospheric correction (Sun and Pinker, 2003). The algorithms for the day and night time reads:

For the day time:

$$T_s = a_o + a_1 T_{10.8} + a_2 (T_{10.8} - T_{12.0}) + a_3 (T_{3.9} - T_{8.7}) + a_4 (T_{10.8} - T_{12.0})^2 + a_5 (\sec \theta_v - 1) + a_6 T_{3.9} \cos \theta_s \quad (4-26)$$

For the night time:

$$T_s = a_o + a_1 T_{10.8} + a_2 (T_{10.8} - T_{12.0}) + a_3 (T_{3.9} - T_{8.7}) + a_4 (T_{10.8} - T_{12.0})^2 + a_5 (\sec \theta_v - 1) \quad (4-27)$$

Where

T_s	= surface temperature	[K]
T_i	=brightness temperature	[K]
θ_v	=satellite view angle	[rad]
θ_s	=solar zenith angle	[rad]
a_i	= the i^{th} regression coefficient determined based on the surface type	[-]

The solar zenith angle correction (θ_s) for the MIR $3.9\mu\text{m}$ is included in the day time since this channel contains solar signals during the day time. a_i are the regression coefficients dependent on surface types. The emissivity effects are now considered through the surface type. Sun and Pinker (2003) demonstrated that using land cover types instead of the traditional surface emissivity helps to reduce the LST retrieval errors. The coefficient for water surface is given below in Table 4-1.

Table 4-1: Coefficients for four channel algorithm(Sun and Pinker, 2007).

coefficients	Day time	Night time
a_o	-29.2629	-20.8035
a_1	1.1054	1.0907
a_2	2.2502	1.8823
a_3	0.1322	0.3357
a_4	0.1889	0.2987
a_5	464.1204	350.8949
a_6	5.75E-05	---

4.3.2. Solar zenith angle and satellite view angle

The solar zenith angle (θ_s) and the satellite view angle (θ_v) are among the factors that influence the magnitude of irradiance reaching the Earth's surface and the radiance received at the satellite respectively. These angles are an input for the surface temperature retrieval algorithm developed by sun and pinker (2007). The solar zenith angle is accounted for the correction radiance at $3.9\mu\text{m}$ and the view angle has an effect on the water leaving signals. This is because the attenuation and augmentation that takes place varies with the distance travelled towards the sensor. the satellite view angle for the pixel at the centre of Lake Tana is calculated to be 6.1° (Alemseged, 2010). The solar zenith angle is calculated as:

$$\theta_s = A \cos(\sin(\pi/180 \times L) \times \sin(\pi/180 \times \delta) + \cos(\pi/180 \times \delta) \times \cos(\pi/180 \times L) \times \cos(\pi/180 \times \omega)) \times 180 / \pi \quad (4-28)$$

Where L =local latitude [°]
 δ = Solar declination [°]
 ω = hour angle [°]

5. IN SITU DATA ANALYSIS AND RESULTS

From the measured in situ data the most complete data set is the measurement for the first day of the field campaign. Therefore time series data which is collected starting from 15th of September 2011 at 16:40 hour to 16th of September 2011 at 17:20 hour is chosen for the in situ data analysis. The analysis, result and discussions are presented as follows:

5.1. Water heat flux

The temperature measurements are performed at 5 minute interval. The sharp drop down of the measured temperature is caused due to the resolution of the sensors (0.4°C). Since measurements showed relatively large variation over consecutive time steps (see Figure 5-1), measurements are aggregated to represent hourly mean temperature (see Figure 5-2).

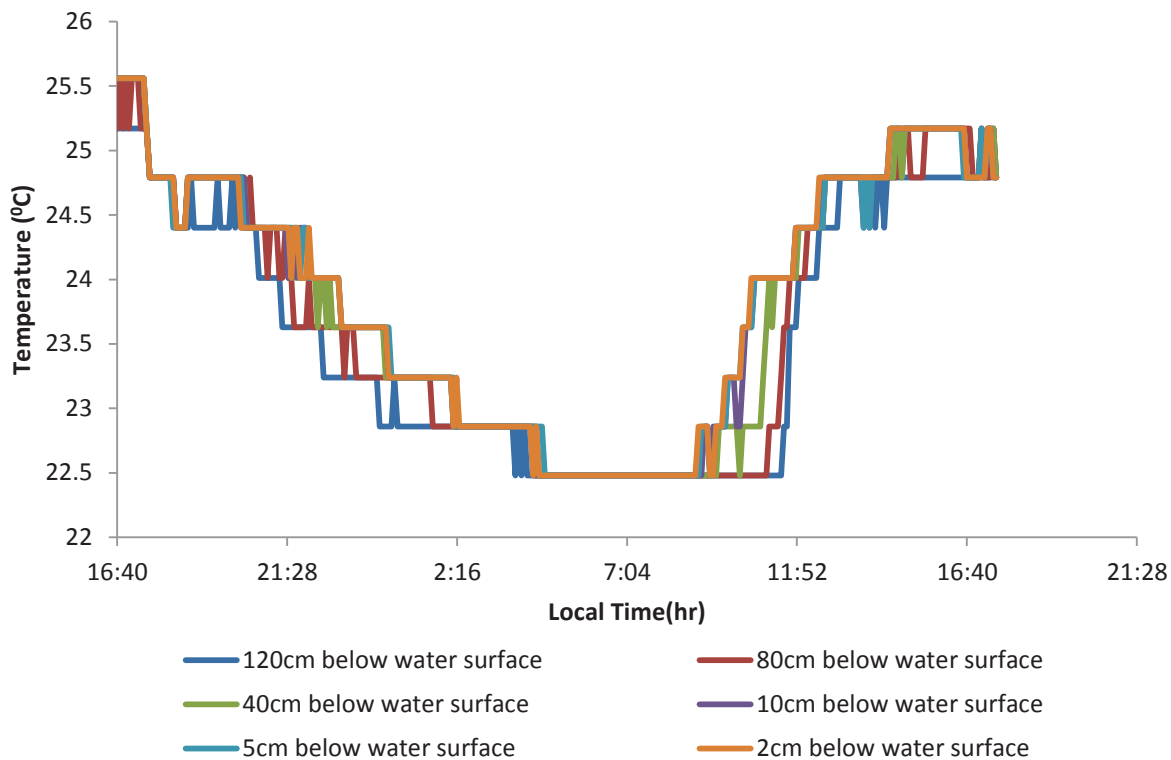


Figure 5-1: Temperature profile of the water (5 minute interval) (Date: 15/09/2011, 16:40hr-16/09/2011, 17:30hr)

The temperature decreases between afternoon and mid-night and is constant until the sun-rise and increases rapidly from the morning to the mid-day. In the afternoon period it is somewhat constant.

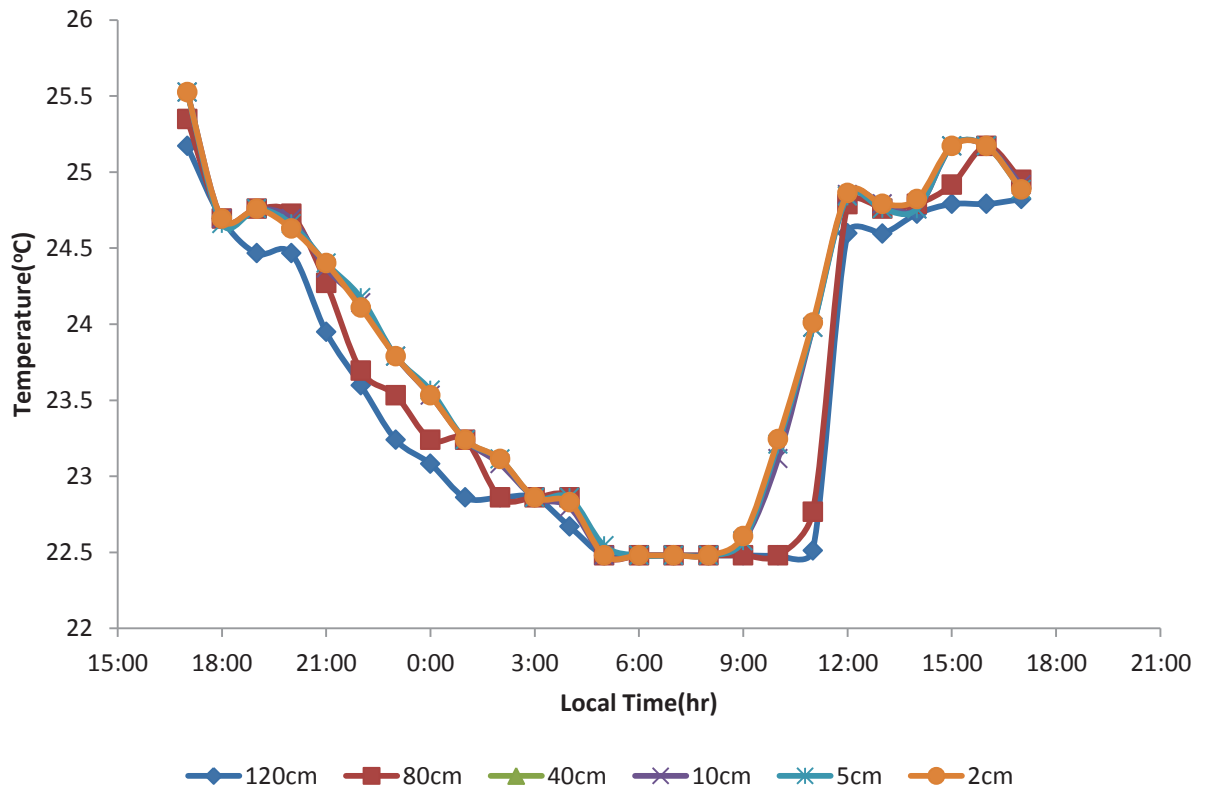


Figure 5-2: Hourly water temperature distribution over time for respective measurement depths (Date: 15/09/2011, 1700hr-16/09/2011, 1700hr)

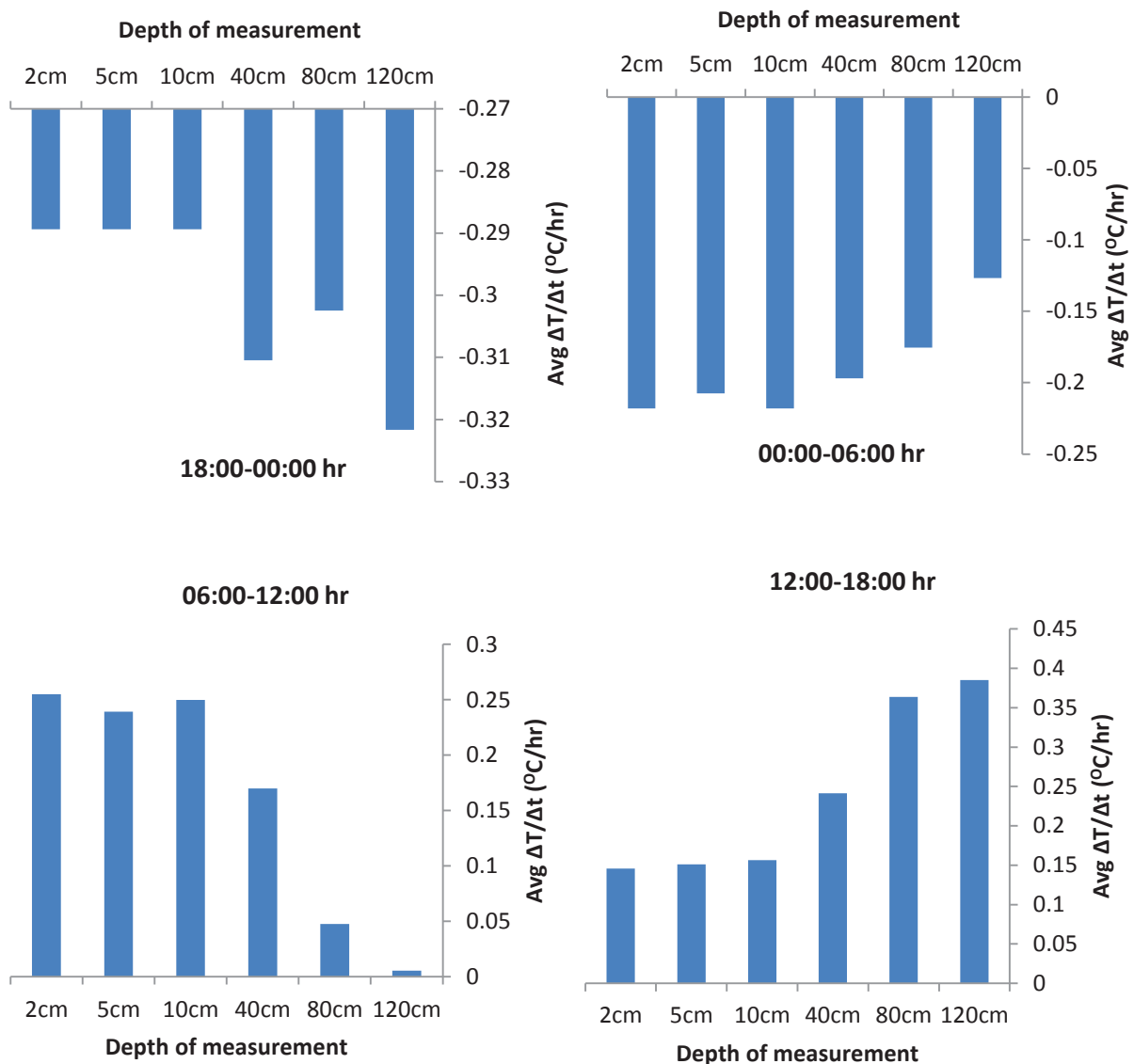


Figure 5-3: The average of the hourly change in temperature ($\Delta T/\Delta t$) for a 6hr time period for the respective depth of measurement (Date: 15/09/2011, 18:00hr-16/09/2011, 17:00hr local time)

During the time period of 18:00-00:00 hours the change in temperature over time ($\Delta T/\Delta t$) for the first three measurement depths (2, 5 and 10cms) is constant with depth. For the remaining depths of measurement (40, 80 and 120cms) the $\Delta T/\Delta t$ is observed to vary and at the 80cm measurement depth the $\Delta T/\Delta t$ is even smaller as compared to the 40cm and 120cm depths. There is also an abrupt increase in $\Delta T/\Delta t$ from 10cm to 40cm measurement depths.

During the time period of 00:00-06:00 hours for the depths of 2, 5 and 10cms the $\Delta T/\Delta t$ is larger in comparison with the other measurement depths and starting from 40cm to 120cm $\Delta T/\Delta t$ shows a decreasing trend.

For the time period of 06:00-12:00 the $\Delta T/\Delta t$ in the first three measurement depths (2, 5 and 10cms) is fairly constant and large. But for the remaining measurement depths (40, 80 and 120cms) there is large difference in $\Delta T/\Delta t$. At the 120cm depth the change is very small as compared with the other measurement depth.

For the time period of 12:00-18:00 hours the $\Delta T/\Delta t$ of 2, 5 and 10cms depths of measurement is almost constant with depth and small as compared with the other depths of measurement. Also $\Delta T/\Delta t$ at the depths of 40, 80 and 120cms increases with depth, and the values are higher than at the other measurement depths.

Generally starting from the afternoon up to the mid-night the $\Delta T/\Delta t$ increases with the depth i.e. the $\Delta T/\Delta t$ is larger at 120cm than the surface. From the mid-night time to the sun rise the $\Delta T/\Delta t$ is larger at the surface than the 120cm, even though the water is cooling. Starting from the sun rise to the mid-day $\Delta T/\Delta t$ is higher at the surface while from the mid-day to the sunset the change is lower at the surface than along the depth of the water. At the day time the water is warming-up and at the night time the water is cooling-down.

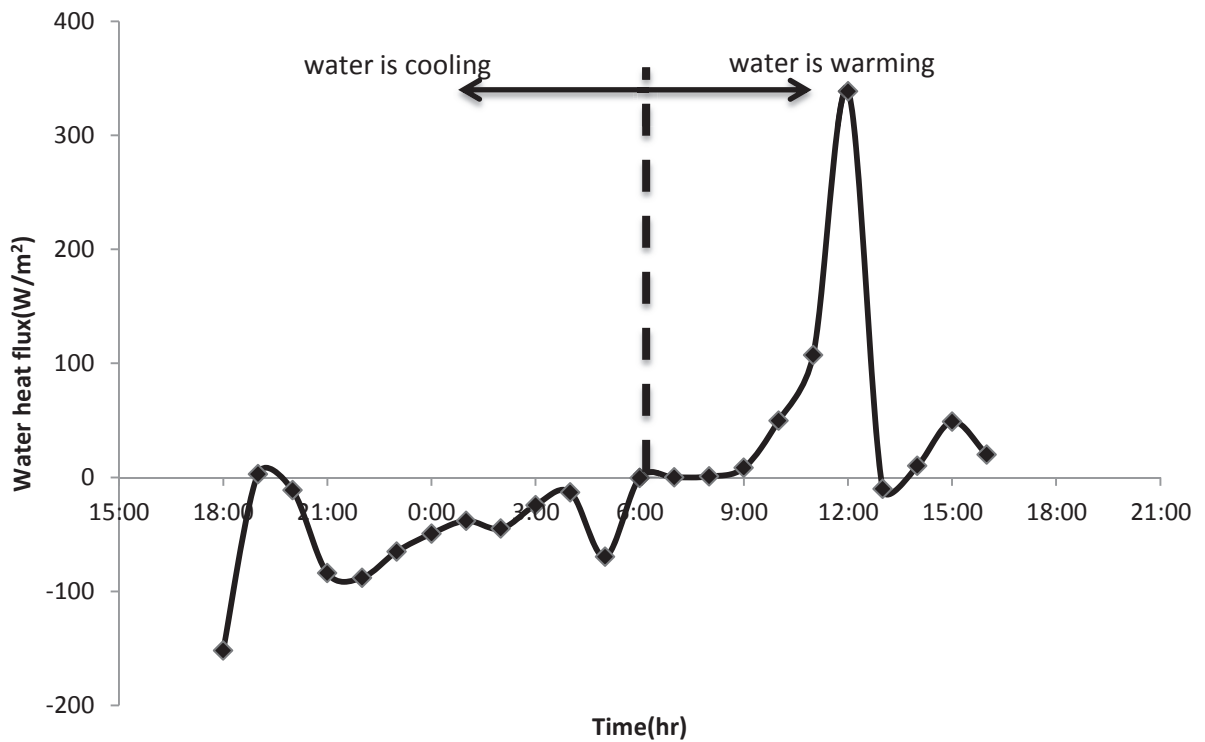


Figure 5-4: Water heat flux with averaged temperature data (Date: 15/09/2011, 18:00hr-16/09/2011, 17:00hr)

The instantaneous water heat flux (G) is calculated from the measurement of temperature profile at different depths using Eq4-6.

The water heat flux is negative starting from in the afternoon which indicates the water is cooling and then starting from the morning time it increases and become positive indicating the warming up period of the water. For the calculation of the water heat flux the temperature of the lake water below 3m depth is assumed to be constant since the measurement at 120cm is assumed to represent up to 3m. Also the heat change is only considered to be in the vertical direction and the horizontal heat exchange is ignored.

During the field campaign period it was raining in the afternoon and the sky is covered by cloud in Lake Tana areas. Therefore the water heat flux computed at the 18:00, 05:00 and 13:00 hours of local time is presumably the effect of the rain.

For the estimation of the water heat flux there must be a detailed data of temperature spatially as well as temporally. Even though it is quite difficult to satisfy the need of spatial coverage, effort is made for the temporal coverage which needs 24 hour coverage at different depths.

5.2. Net radiation

The net radiation is calculated by using Eq.4-7. Since Albedo for the Lake is not measured at the field the outgoing short wave radiation is calculated by taking an Albedo value of 0.1 from the previous work (Abreham Kibret, 2009). The measured surface temperature and air temperature were used to calculate the outgoing and incoming long wave radiations respectively. Figure 5-5 shows the different component of the net radiation and their pattern throughout the period of 24 hours and figure 5-6 shows the behavior of the net radiation for the same period of analysis.

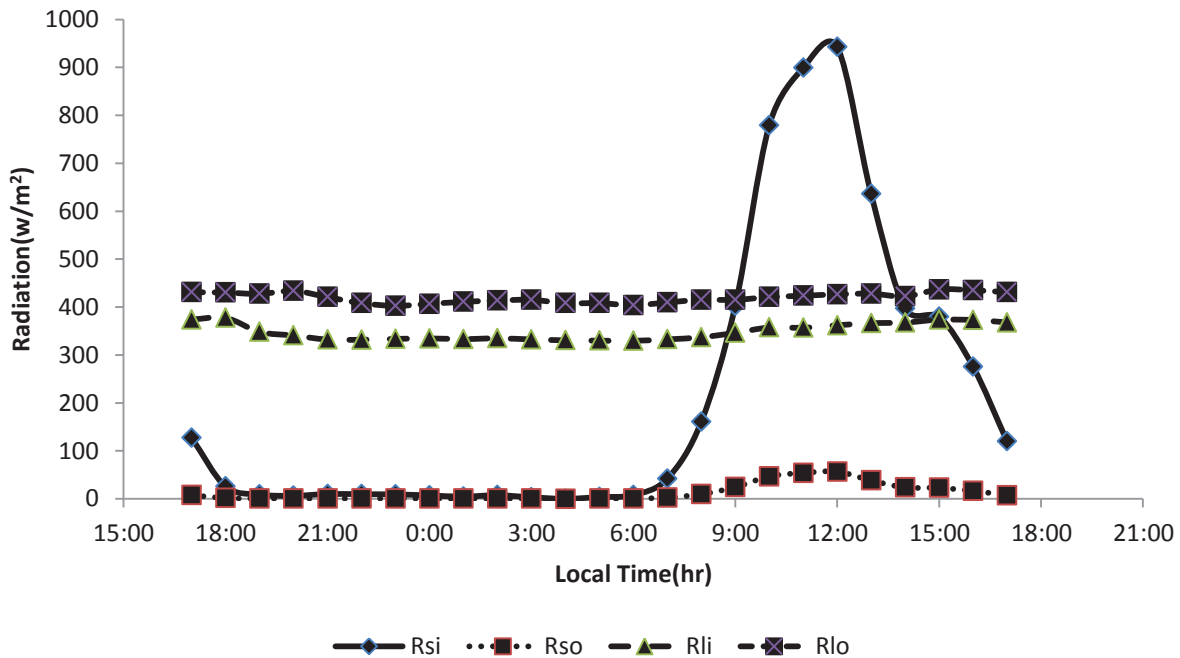


Figure 5-5: Different component of the radiation (Date: 15/09/2011, 17:00hr-16/09/2011, 17:00hr)

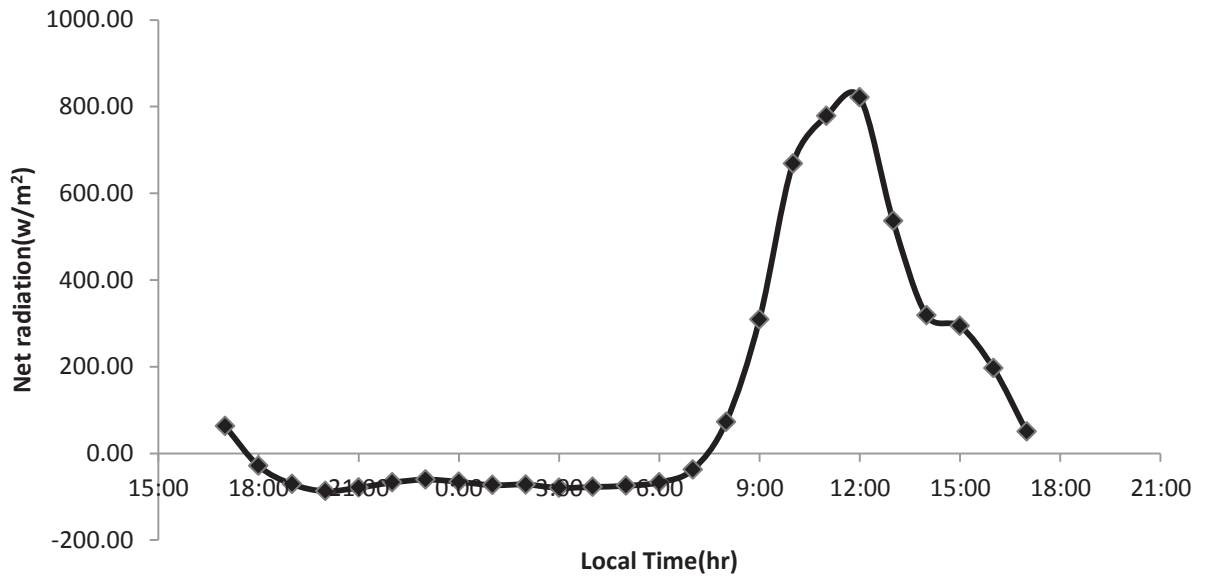


Figure 5-6: Diurnal cycle of net radiation (Date: 15/09/2011, 17:00hr-16/09/2011, 17:00hr)

The net radiation is mostly affected by the short wave radiation since the long wave radiation is mostly constant throughout the observed time. At the night time the net short wave radiation is smaller than the net long wave radiation and the total net radiation become negative.

5.3. The sensible heat flux

The sensible heat flux is the exchange of heat through air as a result of a temperature gradient between the surface and atmosphere. In this study the sensible heat flux determined from Eq. 4-11 and figure 5-7 shows the diurnal cycle of the sensible heat flux.

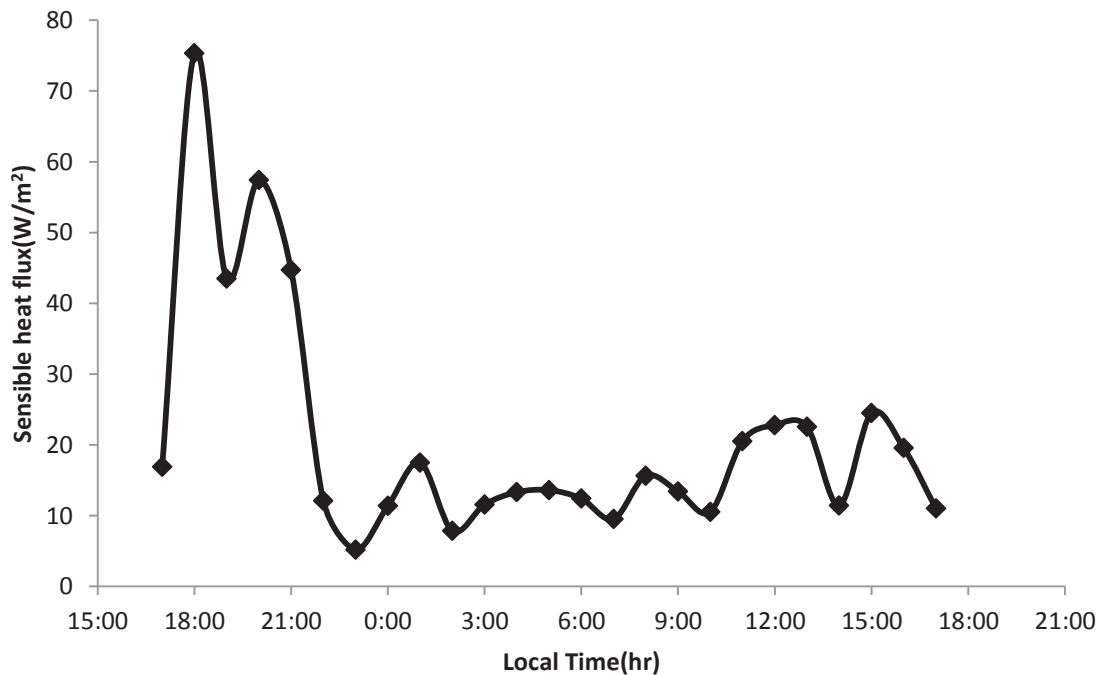


Figure 5-7: Diurnal cycle of Sensible heat flux (Date: 15/09/2011, 17:00hr-16/09/2011, 17:00hr local time)

The sensible heat flux is strongly correlated with the wind speed which is inversely related to the aerodynamic resistance (r_{ah}). The highest value of sensible heat flux (75.33w/m^2) is found due to the very high wind speed recorded at the time (18:00hr).

5.4. Diurnal cycle of evaporation

In this study the latent heat flux is calculated using the Bowen ratio, the Bowen ratio/energy balance (BREB), the energy balance and the Penman methods. The result found in each method is presented in the figure 5.9.

5.4.1. The Bowen ratio method

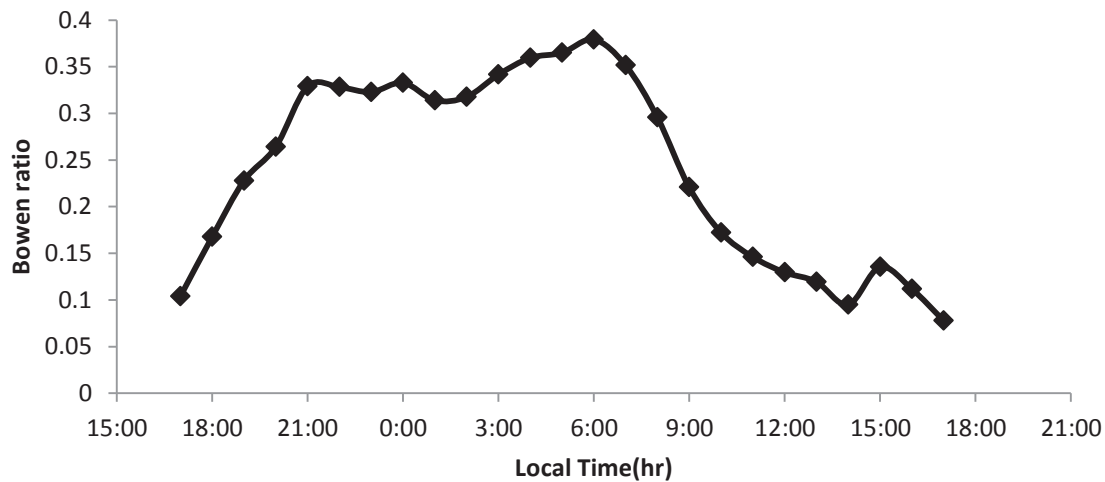


Figure 5-8: Diurnal cycle of Bowen ratio (Date: 15/09/2011, 17:00hr-16/09/2011, 17:00hr)

Figure 5-8 shows the distribution of the Bowen ratio throughout the 24 hours period and it is calculated using Eq.4-14. The Bowen ratio is increasing starting from the sunset and attains its maximum value at the sunrise and decreases during the day time. This is because the temperature difference between the water surface and the air is higher in the night time than the day time while the difference in the vapour pressure acts in reverse fashion. The estimated value of the Bowen ratio ranges between from 0.08 to 0.38.

The estimated value of the latent heat flux by this method follows completely the trends of the sensible heat flux which intern follows the trends of the wind speed. In this method the hourly estimate of latent heat flux has larger value than the other methods for the entire period of the night time.

5.4.2. The Bowen ratio / Energy balance method (BREB)

In this method the latent heat flux is calculated by using Eq.4-13. The major influencing factor in this method is the $(R_n - G)$ term and is independent of the effect of wind. From this term the net radiation affects more the estimate of the Latent heat flux since the water heat flux is small as compared with the net radiation.

5.4.3. The Energy balance method

This method is one of the frequently used methods in the estimation of open water evaporation (Ahmed, 1999). The energy balance procedure as applied to lakes is based upon the conservation of energy principles. The latent heat flux is computed as residual term since the other components are estimated independently and is given by Eq.4-5.

5.4.4. The Penman combination method

The Penman combination method requires the measurement of air temperature, relative humidity, wind speed and net radiation. Except the net radiation, which is calculated from the measurement of incoming short wave radiation, the other parameters are measured directly using field instruments (see section 3-2).

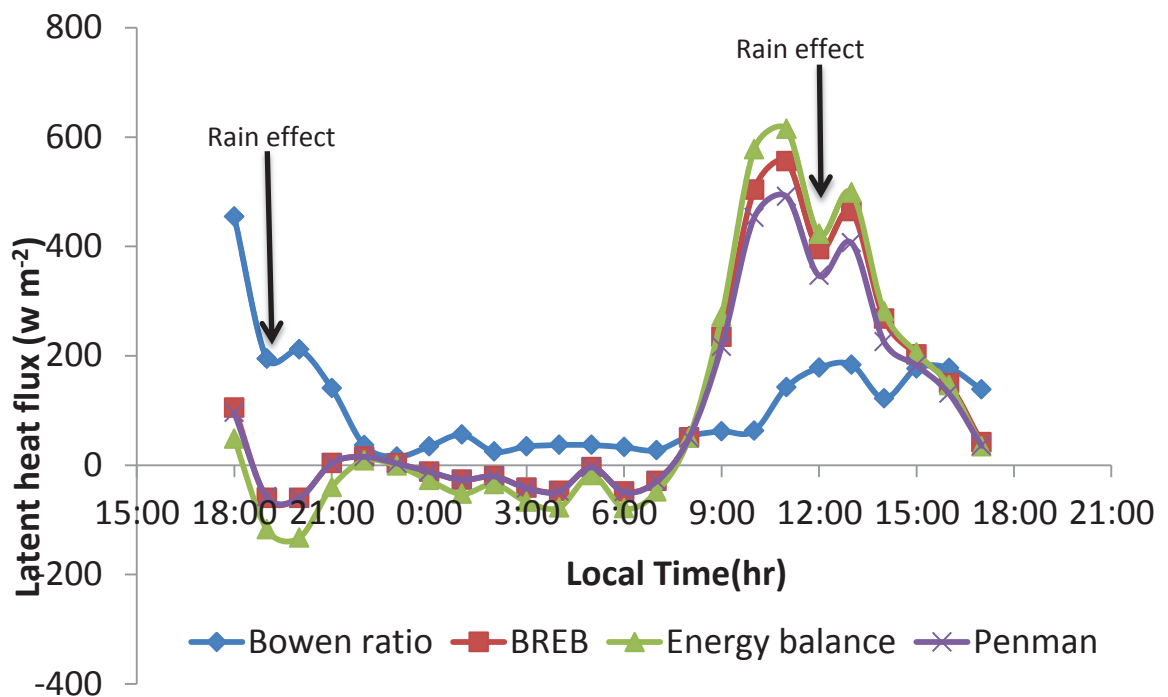


Figure 5-9: Diurnal cycle of latent heat flux with different methods (Date: 15/09/2011, 18:00hr-16/09/2011, 17:00hr)

At 19:00 hour of the first date and 11:00 hour of the second date of measurement the observed rain has an effect in the computed latent heat flux. Webster et al (1996) has shown in their study of the relation between the clouds, radiation and the diurnal cycle of sea surface temperature that a local events of short duration of precipitation can leave a local cooling signature at the surface of the water.

There is a relatively high variability in the latent heat flux during the day time due to the higher change in water heat flux and net radiation through the period of time. During the night time the latent heat flux is observed to have mostly negative value. This is because the water is cooling and also the possibility of the formation of dew.

5.4.5. Comparison of the latent heat flux in the four methods

Figure 5-9 shows the results for the four methods that are applied for the computation of the latent heat flux. The Bowen ratio/ energy balance (BREB), the energy balance and the Penman methods have a

relatively similar pattern while the Bowen ratio method has a different pattern. The similarity in the three methods is presumably resulted from the inclusion of the $(R_n - G)$ term in the equations of the latent heat flux. The pattern of the latent heat flux estimated by the Bowen ratio method has resulted from its dependency on the sensible heat flux and also it doesn't use the $(R_n - G)$ in the computation. The $(R_n - G)$ term is more influencing the change in the latent heat flux and the sensible heat flux is observed to have a relatively less influence for daily estimates. For the hourly estimation of the latent heat flux the water heat flux has an effect in contrary, for the daily estimate it is very small and even can be neglected. The estimated value of evaporation is presented in Table 5-1 below.

Table 5-1: Daily estimate of evaporation (Date: 15/09/2011, 18:00hr-16/09/2011, 17:00hr)

	Bowen ratio	BREB	Energy balance	Penman
Average (Wm^{-2})	110.35	109.94	105.40	98.60
Equivalent Evaporation(mm/day)	3.89	3.88	3.72	3.48

Table 5-2: Daily average of the component of energy balance

	Sensible heat flux	net radiation	Water heat flux
Heat flux (Wm^{-2})	21.00	120.82	-2.72

In the daily cycle of the evaporation, the net radiation is the only input to the energy balance and it is larger than the other component. The water heat flux is observed to have the smallest value for the daily estimate. Generally the net radiation is the most dominant parameter (see Table 5-2) followed by the sensible heat flux and the water heat flux is least one in the daily estimate of the latent heat flux.

6. REMOTE SENSING DATA ANALYSIS AND RESULTS

6.1. Net radiation

Net radiation is the difference between the incoming and outgoing radiation flux of both the short and long wavelength range at the surface of the earth. Remote sensing offers a high spatial and temporal coverage of the land surface parameters which are difficult to measure at the ground. In this study the incoming short and long wave radiation are directly downloaded from the LSA SAF product dissemination site (<http://landsaf.meteo.pt/>). The product is atmospherically corrected.

The earth surface albedo is an important parameter to estimate the net short wave radiation. The MODIS albedo product (MCD43A3) provides 500-meter data describing both directional hemispherical reflectance (black-sky albedo) and bihemispherical reflectance (white-sky albedo). The MCD43A3 product contains 16 days of data provided in a level-3 gridded data set in Sinusoidal projection (see the product user manual). The product is downloaded from the web site

https://lpdaac.usgs.gov/products/modis_products_table/albedo/16_day_13_global_500m/mcd43a3.

For this study the total albedo is computed from eq.4-25 and the albedo map of the Lake Tana area is presented in figure 6-1.a.

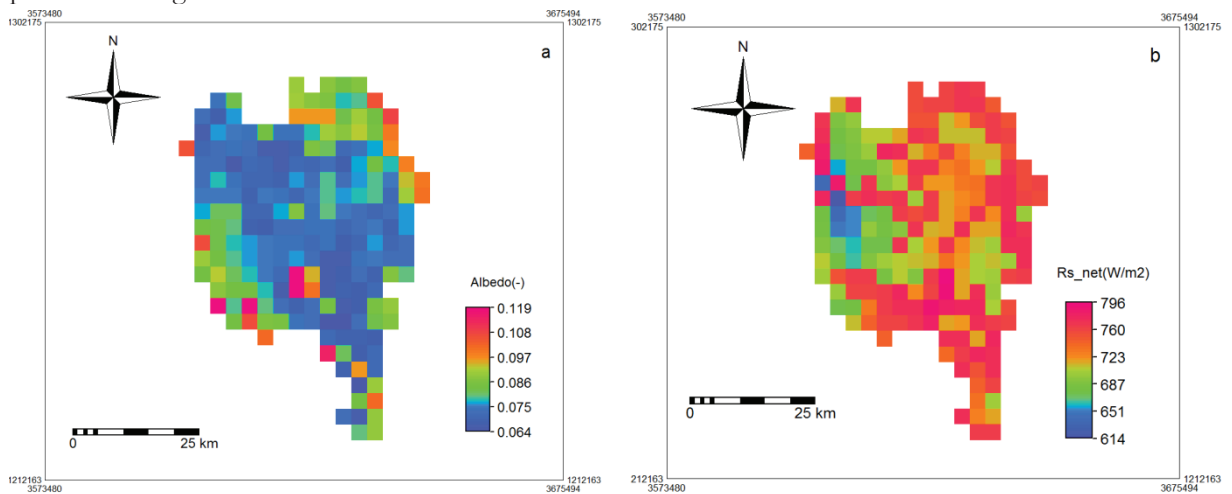


Figure 6-1: Total albedo of Lake Tana area (a) (15th of September 2011) and instantaneous net short wave radiation ($W\ m^{-2}$) (16th of September 2011 at 10:00 hour local time) (b)

The albedo of the lake water is directly related to the composition of the water and the depth of the water. From figure 6-1a it is observed that the albedo of the lake surface ranges from 0.064 to 0.119. Higher value of albedo indicates a relatively higher turbidity and/or shallowness of the lake while lower value of albedo indicates a relatively lower turbidity and/or depth of the lake. For the ground measurement point the albedo value is 0.08. Higher value of albedo of 0.119 is observed near the centre of the lake which is presumably the effect of the island in the lake and at north eastern part of the lake also higher value of albedo observed is presumably due to shallower lake depth (see figure 3-2: depth of Lake Tana) and the shore effect.

The incoming short wave radiation used in this study is the LSA SAF product of the down-welling surface short-wave radiation flux (DSSF) which has a 30-minute temporal resolution. The outgoing short wave radiation is calculated from Eq.4-22 and the net short wave radiation is calculated using eq.Eq.4-21. The lowest value of net short wave radiation (614W m^{-2}) observed in the western part of the lake due the cloud cover at the time. The net short wave radiation for 16th of September 2011 at 10:00hr is presented in figure 6-2 below.

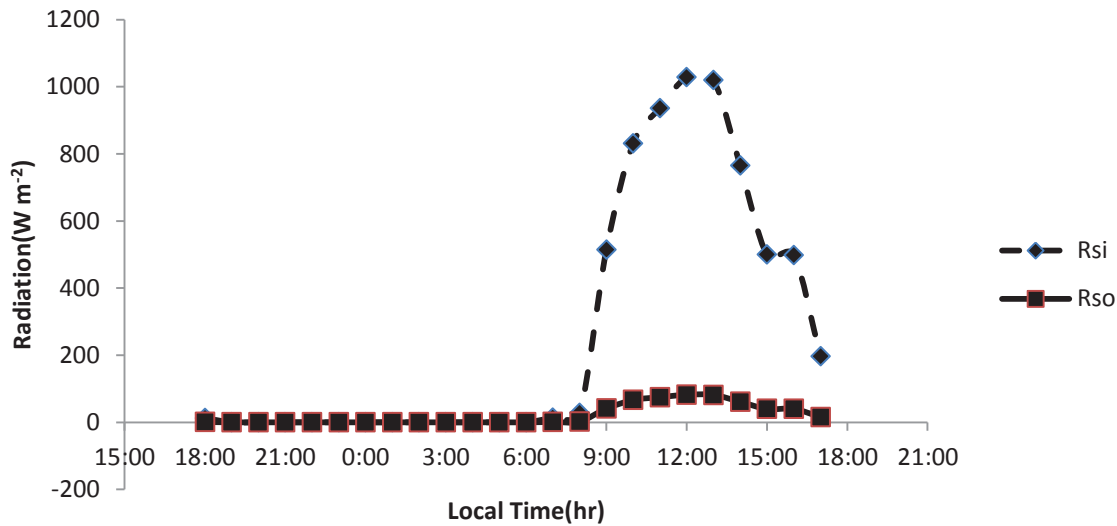


Figure 6-2: The incoming and outgoing short wave radiation from the remote sensing data (from 15th of September 2011 at 18:00hr to 16th of September 2011 at 17:00hr).

From figure 6-2 it is seen that at 15:00hr the incoming short wave radiation is presumably affected by the cloud.

The difference between the incoming long wave radiation from the atmosphere and the outgoing radiation that is emitted from the lake surface is the net long wave radiation. The incoming long wave radiation used in this study is the LSA SAF product of the down-welling surface long-wave radiation flux (DSLRF). The outgoing long wave radiation (R_{lo}) is estimated from the remote sensing data of surface temperature of the water and the emissivity value of 0.9744 found from the in situ data. The emissivity of the lake is assumed to be the same throughout the entire lake area and the 24 hours. For the calculation of the long wave outgoing radiation the surface temperature of the water is retrieved from the MSG/SEVIRI and Eq. 4-18 is used and the surface temperature is retrieved using the four channel algorithm.

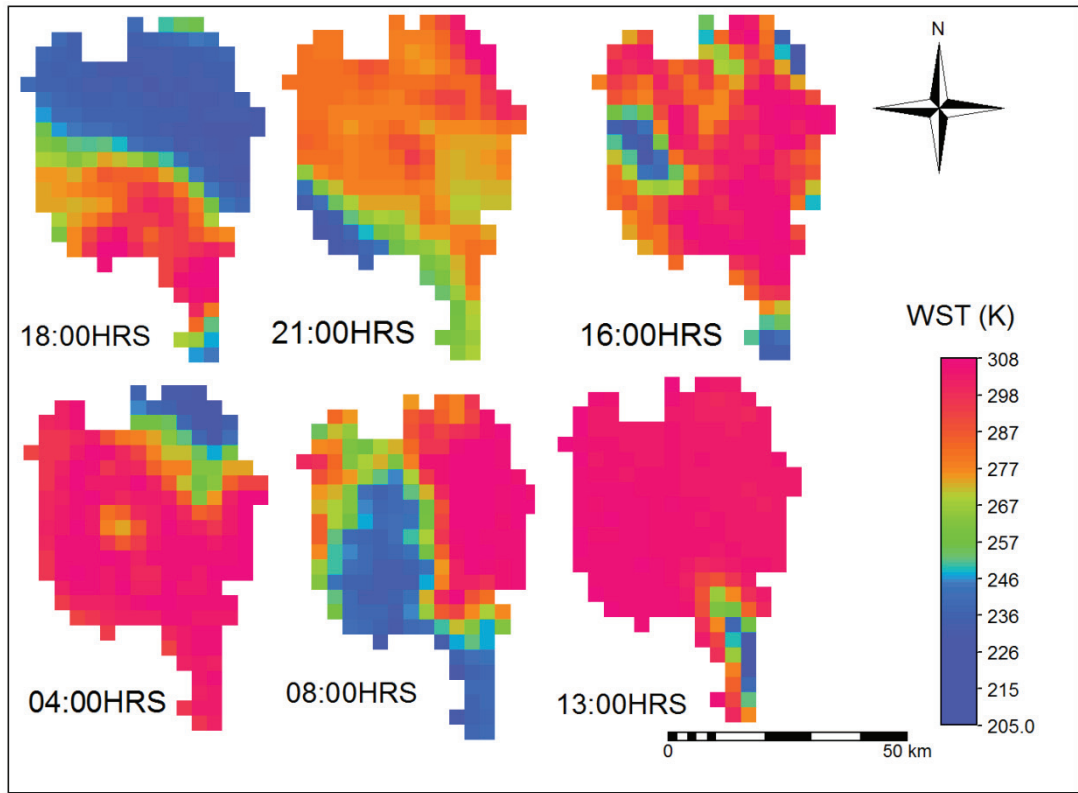


Figure 6-3: Time series map of cloud affected water surface temperature

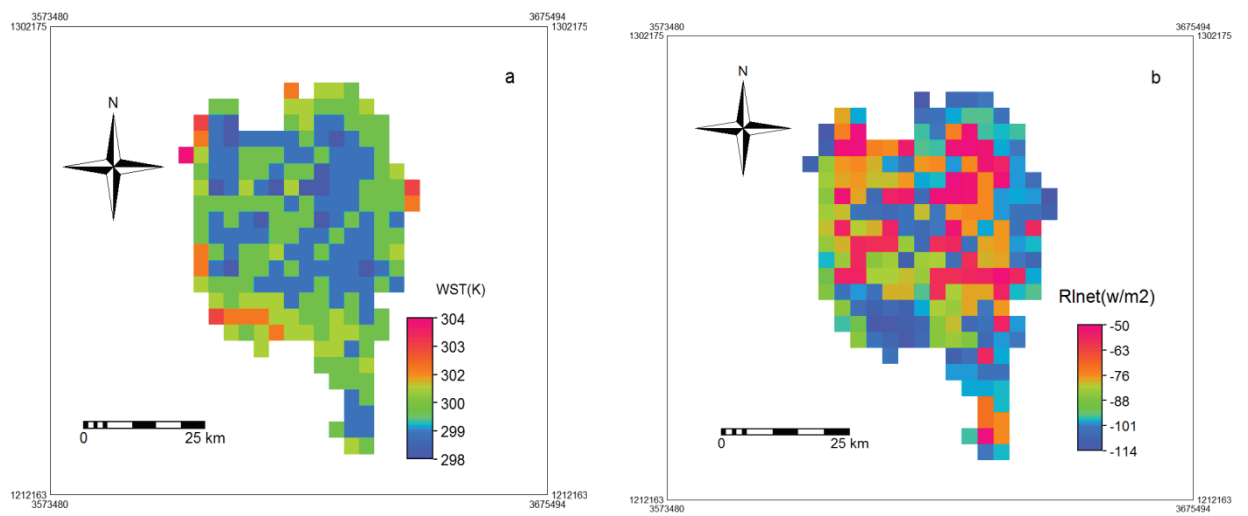


Figure 6-4: Surface temperature of water (K) (a) and net long wave radiation ($W m^{-2}$) (b) of the 16th of September 2011 at 10:00hr local time

By comparing the spatial distribution of the water surface temperature (WST) and the net long wave radiation from figure 6-4a and 6-4b it can be concluded that the net long wave radiation follows the trends of the water surface temperature i.e. those areas which has lowest value of the surface temperature has also the lowest net long wave radiation and vice versa.

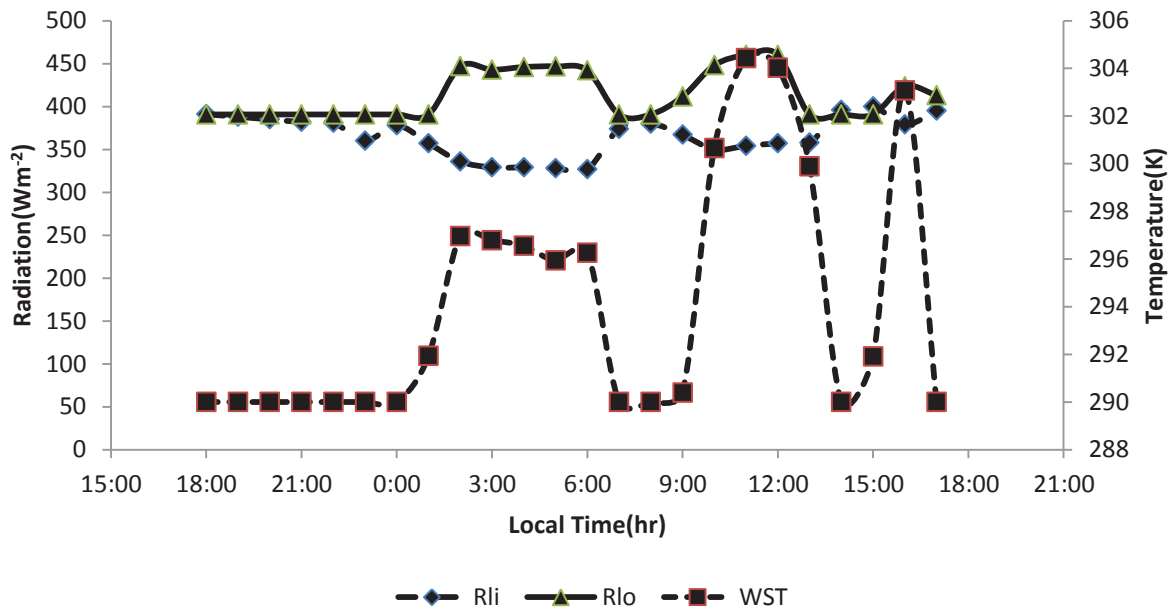


Figure 6-5: Diurnal cycle of incoming long wave (Rli) and outgoing long wave (Rlo) radiation (from 15th of September 2011 at 18:00hr to 16th of September 2011 at 17:00hr local time) combined with surface temperature(WST) for a pixel having ground measurement

A nearly constant value of outgoing long wave radiation (Rlo) (391 Wm^{-2}) was obtained for the time period from 18:00hr of 15th of September 2011 to 00:00hr of 16th of September 2011 and for 07:00, 08:00, 14:00 and 17:00 hours of the 16th of September 2011(see Figure 6-5). This is presumably due to the surface temperature assigned value in the cloud masking procedure. It is noted that since for this period the retrieved surface temperature is affected by cloud that is masked by giving a 290K temperature value for cloud affected pixels (see Figure 6-3 for cloud effect). It is also seen that the incoming long wave radiation has also been affected by the cloud cover during these periods, since the propagation of the cloud will increase the emissivity of the atmosphere. During the 24 hour period the outgoing long wave radiation follows the trends of the surface temperature of the water.

The net radiation calculation based on the remote sensing data is done using Eq.4-7. The instantaneous value for 16th of September 2011 at 10:00 hour is shown in figure 6-6 and figure 6-7 show the diurnal cycle of net radiation.

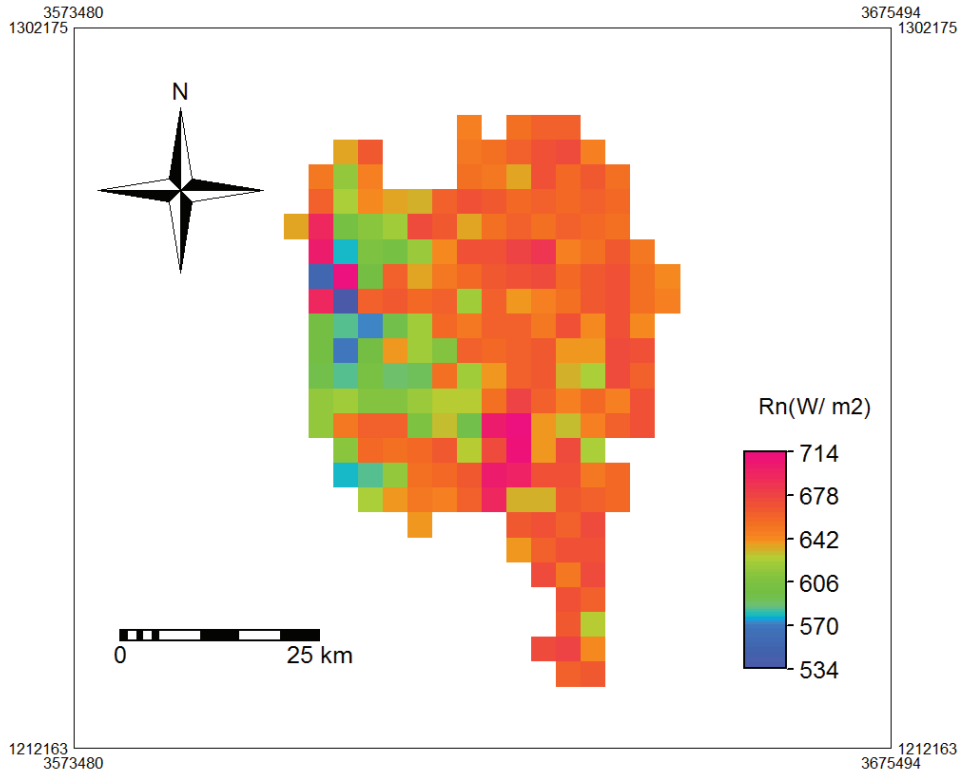


Figure 6-6: Net radiation (Wm^{-2}) at 10:00 hour local time of the 16th of September 2011

Figure 6-6 shows that the spatially distribution of the instantaneous net radiation closely follows the distribution of the net short wave radiation (see also Figure 6-1b). This is because the net short wave radiation has much higher value than the net long wave radiation. Area of the lake which has lowest value net short wave radiation is also observed to have the lowest net radiation and vice versa.

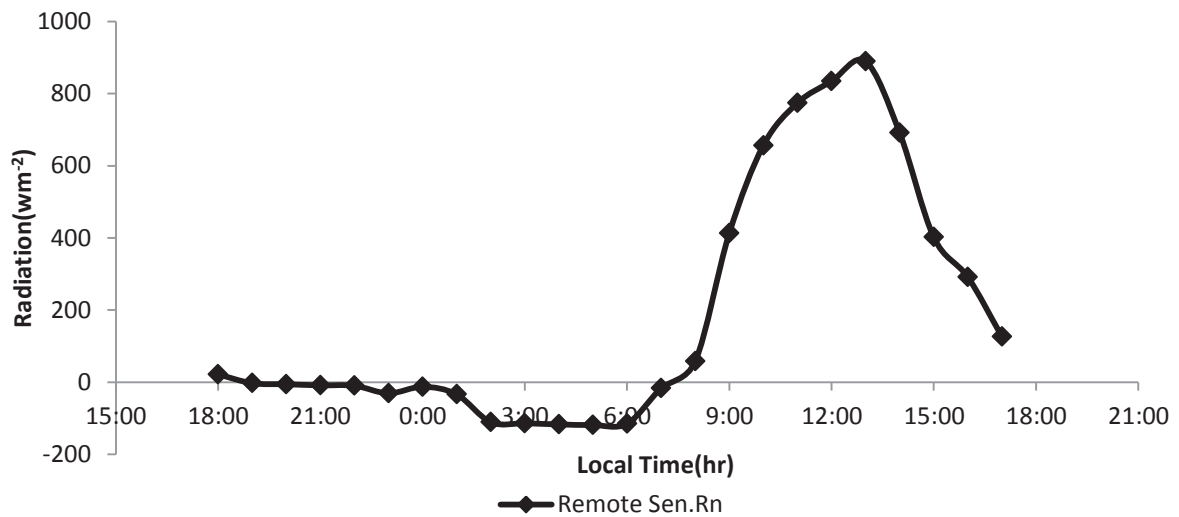


Figure 6-7: Diurnal cycle of net radiation (from 15th of September 2011 at 18:00hr to 16th of September 2011 at 17:00hr)

The comparison of made between figure 6-7 and figure 6-2 suggests that the diurnal cycle of the net radiation follows the diurnal cycle of the incoming short wave radiation, since the albedo is assumed to be constant throughout the 24 hours.

6.2. Water heat flux

Since the retrieved surface temperatures for the date that the ground measurement is done were highly affected by cloud cover, it is quite difficult to estimate the water heat flux from the retrieved water surface temperature. This is because of the cloud masking which assigns the cloud covered pixels a fixed value of 290k. Therefore, it is difficult to estimate the water heat flux from the remote sensing data and time constraint for the study the water heat flux calculated from the in situ measurement is taken as a surrogate for the remote sensing data.

6.3. Diurnal cycle of evaporation

The estimation of latent heat flux is made by using the net radiation computed from the remote sensing data, the water heat flux computed from the in situ data analysis and the Bowen ratio from the in situ data analysis. In this study Eq.4-13 (the BREB method) is used to calculate the latent heat flux from the remote sensing data. Since the data for the estimation of the evaporation covers a 24 hours cycle, the total daily evaporation is found by simply summing the hourly evaporation values. The sensible heat flux is calculated as a residual term of the energy balance equation using Eq.4-5.

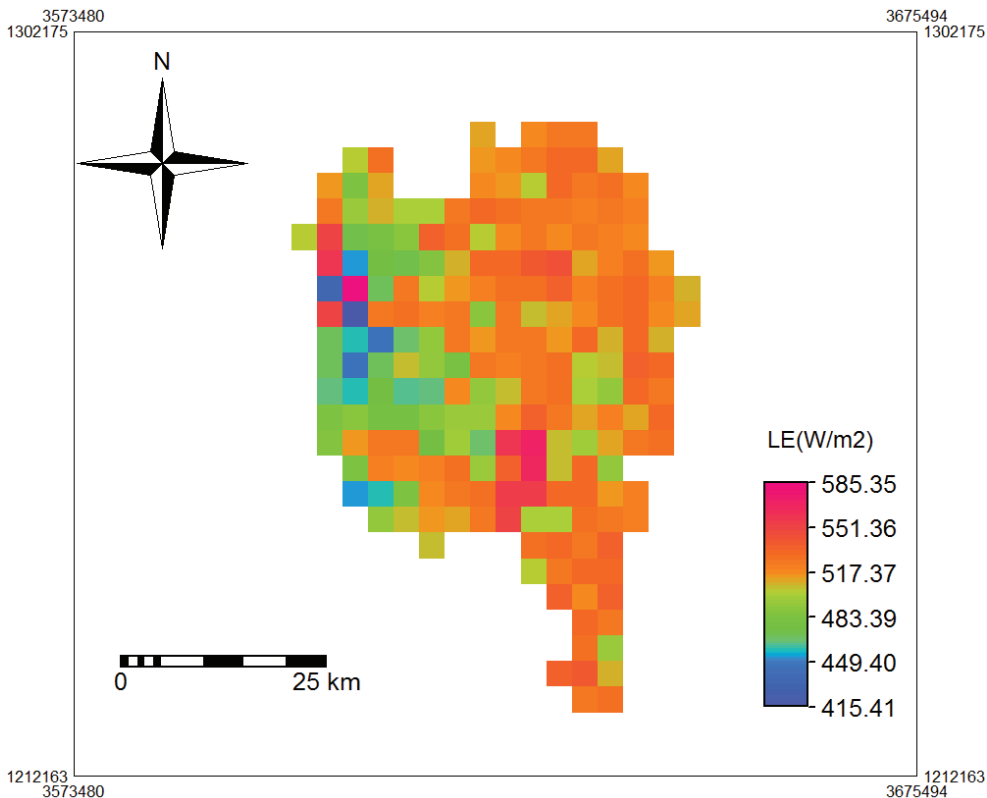


Figure 6-8: latent heat flux at 10:00hr local time of the 16th of September 2011

The main parameter that controls the latent heat flux is the net radiation. Figure 6-8 shows the spatial distribution and at the western part of the lake the latent heat has lowest value suggests the effect of the net radiation which in turn is affected by incoming short wave radiation.

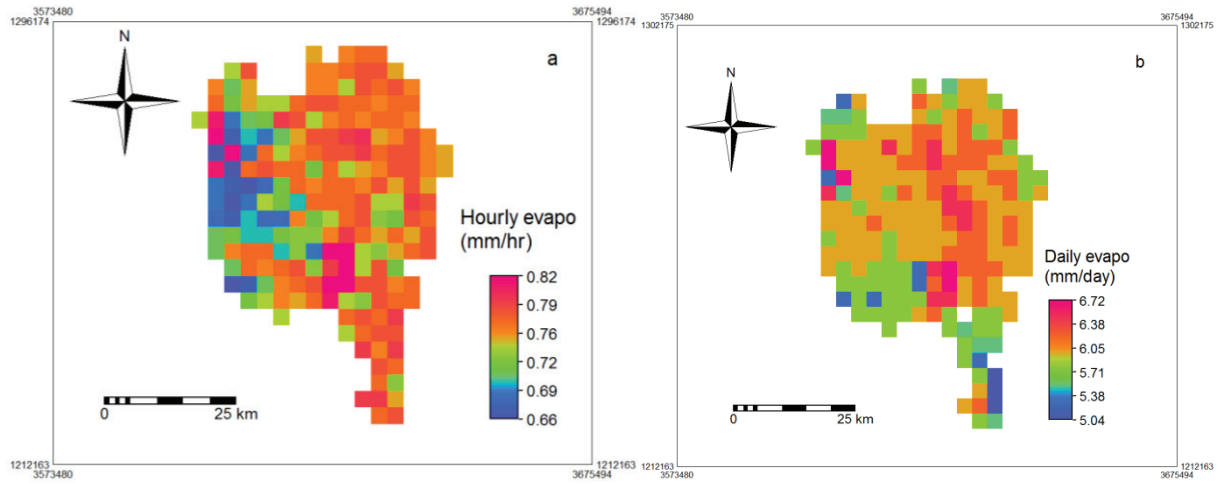


Figure 6-9: Hourly at 10:00hr local time and daily evaporation 16th of September 2011 (a and b respectively)

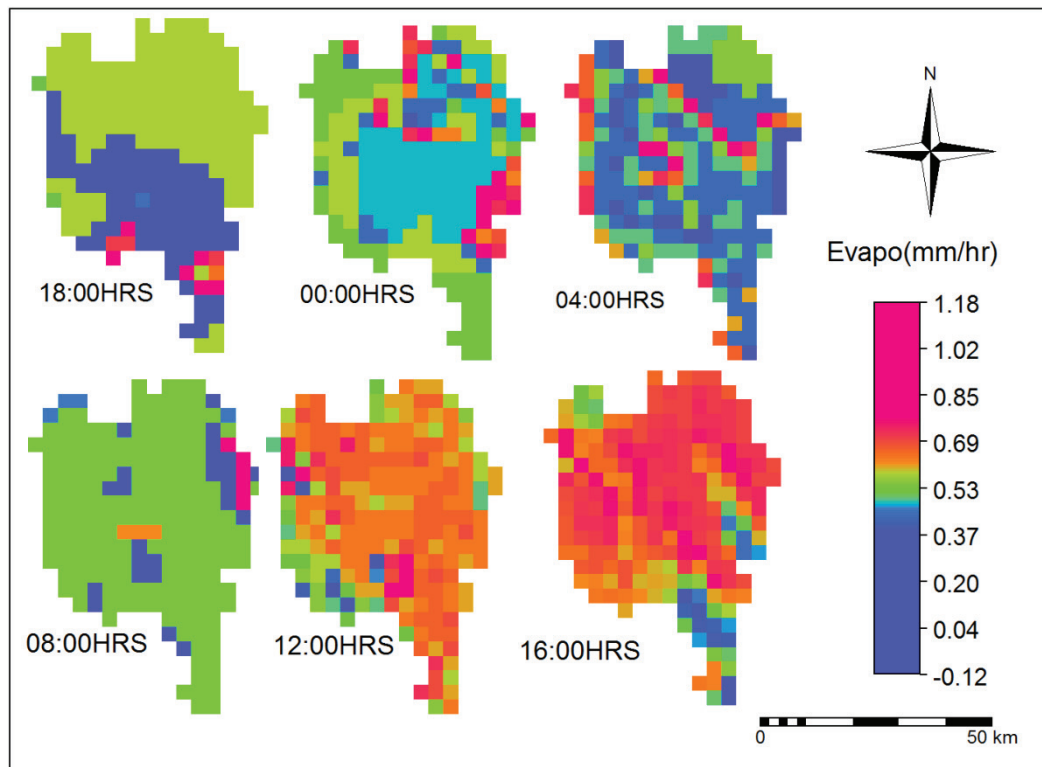


Figure 6-10: Time series map showing the hourly estimate of evaporation

A relatively low value of evaporation of 5.04mm/day (see figure 6-9b) is observed for the areas where the pixels are covered by cloud. From the time series map of the 18:00hr, 00:00hr and 04:00hr the cloud effect

is clearly shown for most part of the lake giving lowest value of evaporation. For the location where the in situ measurement is taken the daily evaporation calculated from the remote sensing data is 5.49mm/day.

Table 6-1: Parameters affecting the estimate of evaporation

item	Equation used	Affecting parameter	Remark
Latent heat flux	$\lambda E = \frac{R_n - G}{(\beta + 1)}$	Net radiation Water heat flux Bowen ratio	
Net radiation	$R_n = R_s \downarrow - R_s \uparrow + R_l \downarrow - R_l \uparrow$		
	$R_s \downarrow = (a_s + b_s \frac{n}{N}) R_a$	Cloud cover, sunshine hour	Zero at night time
	$R_s \uparrow = \alpha R_s \downarrow$	Surface albedo and $R_s \downarrow$	
	$R_l \downarrow = \varepsilon_a \sigma T_a^4$	Air temperature and emissivity of air	
	$R_l \uparrow = \varepsilon_s \sigma T_s^4$	Surface temperature and emissivity of water	
Bowen ratio	$\beta = \gamma \frac{[T_2 - T_1]}{[e_2 - e_1]}$	The difference b/n the surface and air temperature The difference b/n the surface and air vapor pressure The psychrometric constant	β maximum at night time

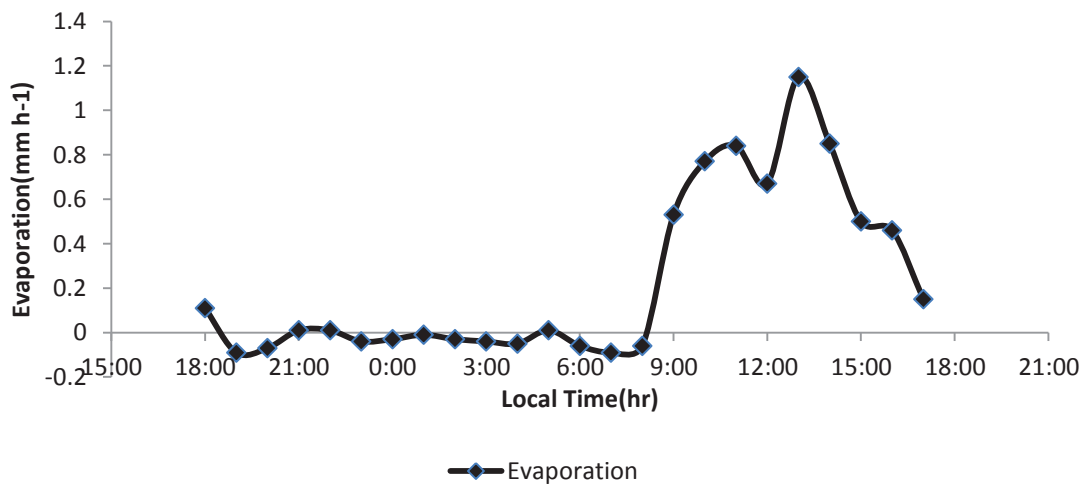


Figure 6-11: Diurnal cycle of evaporation

The process of evaporation completely follows the trends of the latent heat flux which intern follows the pattern of the net radiation. The estimation of evaporation from the remote sensing data combined with the in situ data is done using the Bowen ratio energy balance method (BREB) method which is described by Eq.4-13. The water heat flux and the Bowen ratio estimated from the in situ measurements are taken and assumed to be constant for the whole areas of the lake. Figure 6-10 and 6-11 shows that in the estimates of the evaporation are relatively lower at the night time and larger in the day light hours. The highest value of evaporation at the 13:00hr is the resulted from a relatively large value of net radiation and low value of water heat flux computed at the time. This suggests in the diurnal cycle of evaporation the net radiation and water heat flux are driving force for the process of lake evaporation. Figure 6-10 also shown there is a spatial variability in the lake evaporation in addition to the temporal variability.

6.4. Comparison of Results

6.4.1. Comparison of the remote sensing and in situ measurement

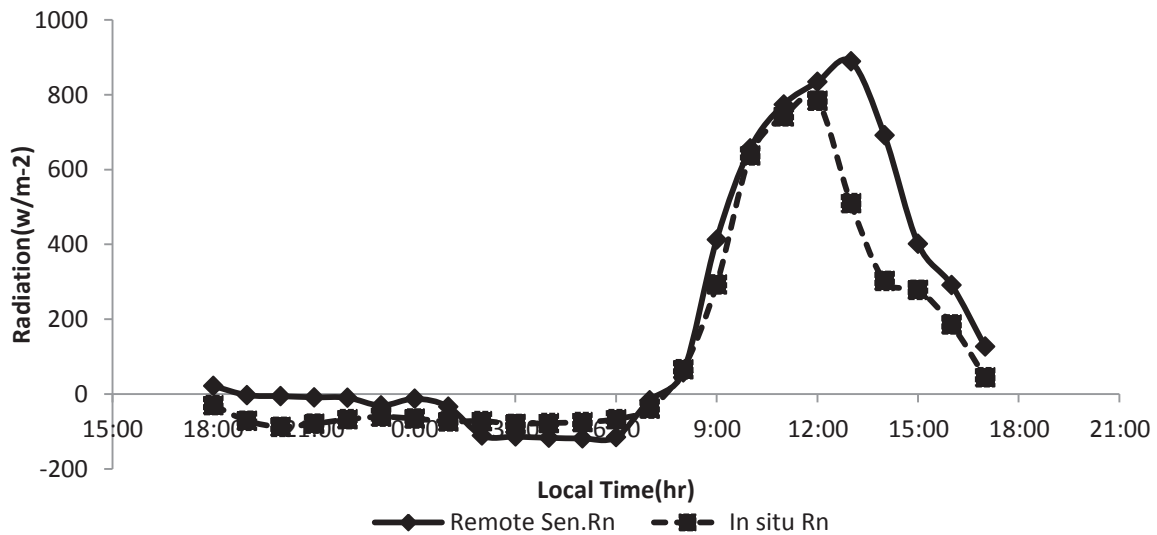


Figure 6-12: Remote sensing and In situ measurement of net radiation ($W m^{-2}$)

The net radiation calculated (see Figure 6-12 above) using the remote sensing data (for the pixel of the in situ measurement) is observed to be higher than the in situ measurement. The main cause for this difference is the value of albedo, which has a direct impact on the calculated outgoing short wave, is 0.1 for the in situ measurement and 0.08 for the remote sensing technique. The in situ measurement for the incoming short wave radiation is taken without calibration of the Pyranometer and most of the components of the net radiation are calculated using empirical relations that require the measurement of the incoming short wave and the water surface temperature. This is the possible reason why the net radiation calculated from in situ data are smaller than that of the remote sensing and it is also possible that the satellite product has some error in clouded conditions, despite that it was atmospherically corrected.

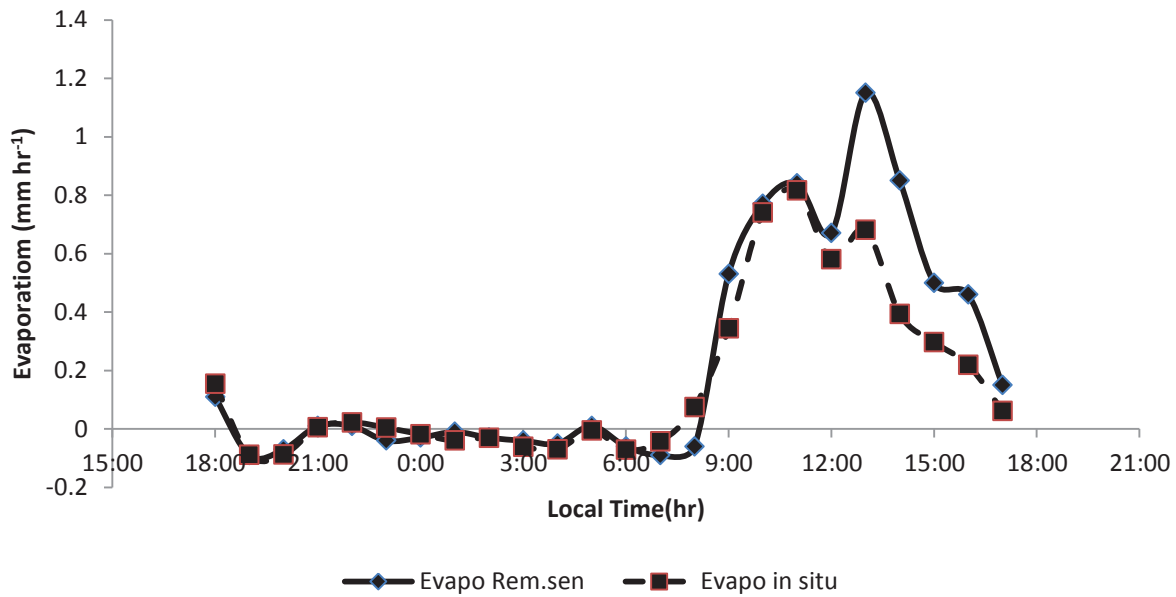


Figure 6-13: Diurnal cycle of evaporation from in situ measurement and remote sensing

From figure 6-13 shows that there is an agreement between the estimates of hourly evaporation with the remote sensing and the in situ data up to 12:00 hours. After this the evaporation estimated is affected by the cloud and also the remote sensing value of albedo (0.08) albedo is lower than that of the in situ (0.1) which is suggested by Alebachew (2009).

Table 6-2: Comparison of average daily flux (all values in $W m^{-2}$)

	Net Radiation		Sensible heat		Water heat	Latent heat	
	RS	In situ	RS	In situ	In situ	RS	In situ
average flux($W m^{-2}$)	202.53	120.82	48.70	21	-2.72	155.55	109.94

6.4.2. Comparison with previous studies

It is very important to make a comparison of the results with the previous studies by investigating the values obtained and the method the studies have applied. For this the studies made by Alebachew in (2009) and Berhanu in (2010) are chosen.

The study undertaken by Berhanu has estimated the evaporation from Lake Tana on monthly basis and here it is converted in to the daily basis for the ease of comparison. He uses five methods which are Hargreaves, Penman (after maidement), Brutsaert-Stricker, CRWE model and CRLE model (refer Berhanu (2010) for the explanation of the methods and models) and the estimated evaporation from the lake is 4.4mm/day, 5.03mm/day, 5.67mm/day, 4.17mm/day and 4.03mm/day respectively using the meteorological station at Bahir Dar.

Table 6-3: Comparison of methods and conditions of measurement

current study	Alebachew (2009)
- The Bowen ratio method is used to estimate H	- Sonic-anemometer is used to measure H
- Only incoming solar radiation is measured by Pyranometer	- Incoming as well as outgoing solar radiation is measured by CNR1 radiometer
- Measurement is made for 24 hours	- Measurement were made for 12 hour
- It is cloudy day	- It was clear day
- Measurement were made at a point	- Measurement were made by travelling with a boat
- Albedo value is assumed to be constant throughout the day	- Albedo value is calculated throughout the day

Table 6-4: The estimated daily evaporation

Evaporation(mm/day)			
This study		Alebachew(2009)	Berhanu(2010)
Remote sensing	In situ	Remote sensing	Remote sensing
5.49	3.88	4.94	5.03

Comparison of estimate of evaporation is made based on the result found using BREB method (refer Eq.4-13). From the results it is seen that the remote sensing method, which uses the water heat flux and Bowen ratio estimate from the in situ measurement, has given a relatively close estimate of evaporation compared with the previous studies.

Comparison of different components of the energy fluxes is made for the instant (11:00 local time) which is close to the time (11:15 local time) that previously Alebachew has calculated the instantaneous values on the 27th of September 2008.

 Table 6-5: Comparison with previous study of Alebachew (2009) (all values in $W m^{-2}$) for 11:00hr local time

	Method	Net Radiation	Sensible heat	Water heat	Latent heat
Alebachew	Remote sensing	791	39	423	315
	in situ	777	44	423	329
This study	Remote sensing	760	82	107	571
	in situ	742	20	107	555

For the estimation of different component of the energy balance terms using the in situ data is made independently for each term. Due to this the energy balance has a closure error of $60 Wm^{-2}$ in this study. The estimate of the net radiation in this study and the in previous study of Alebachew show a close agreement in both the in situ and remote sensing techniques. The sensible heat flux estimate of remote sensing is very high in comparison with the in situ calculated results and from the result of the previous work of Alebachew. The reason for this variation is that the sensible heat flux in this study using the remote sensing method is calculated as a residual term of the energy balance equation and it is not estimated directly. The estimate of the water heat flux and the latent heat flux estimate found in this study vary largely with the previous study of Alebachew. This is because the measurement day (27th of September 2008) is clear sky without rain while for this study the measurement days (15th and 16th of September 2011) are cloudy with rain (see Table6-3). The main point that causes the difference in water

heat and latent heat flux is that at the time (11:00hr) the ground location for Alebachew result is different from this study, since Alebachew has taken the in situ data by travelling with the boat

7. CONCLUSIONS AND RECOMMENDATIONS

7.1. Conclusions

This study applied four methods for assessing the diurnal cycle of the open water evaporation from Lake Tana. The methods include the Penman combination equation, the energy balance, the Bowen ratio energy balance method (BREB) and the Bowen ratio method. The study also involves the assessment of the spatial variability of the open water evaporation of Lake Tana.

From the results the following conclusions are made:

- The Penman combination, the energy balance and the Bowen ratio energy balance (BREB) method has estimated the open water evaporation for the Lake Tana, and a plausible and comparable value which are close to each other were obtained. The Bowen ratio method has shown different trend on the estimated hourly evaporation, especially during the night time by resulting a positive estimate of latent heat flux while the others gives a negative estimate.
- The net radiation flux showed a stable negative value during the night and then increased steadily starting from 06:00hr until 12:00hr and then decreased. The water heat flux has also a negative value at the night time and started to increase from 06:00hr attaining its maximum positive value at 12:00hr and then decreases. The sensible heat flux is observed to have a positive value throughout the 24 hour period. The latent heat flux, following the trends of the net radiation and the water heat flux, has negative value during the night time indicating the formation of dew.
- From the components of the energy balance, the incoming solar radiation is the major source for the evolution the latent heat flux which in turn directly related to the evaporation. In this study the net radiation is observed to have a large effect on the diurnal cycle of evaporation. Cloud cover has an effect on the incoming solar radiation. The water heat flux has shown an effect on estimated hourly evaporation. However, for the daily estimate its effect is very small, suggesting that the energy gained at the day time is lost at the night time. The sensible heat flux has less effect in the diurnal cycle of the open water evaporation.
- There is an agreement between the estimates of hourly evaporation with the remote sensing and the in situ data up to 1200 hours. After this hour, the estimated evaporation is affected by the cloud and also the remote sensing value of albedo (0.08) albedo is lower than that of the in situ (0.1) which is suggested by Alebachew (2009). The daily estimate of the evaporation using the remote sensing data is relatively higher than the estimate made by the in situ data.

7.2. Recommendations

To improve the estimation of the evaporation from Lake Tana the following recommendation are made.

- The spatial variability of evaporation in the lake area clearly indicates the ground measurement should be done in such a way to represent the lake area as much as possible. This helps to avoid/reduce the error that will be introduced in the sampling.
- The instrument that is going to be used for the measurement (radiation, temperature, humidity wind speed and etc.) must be calibrated before the measurement.
- The get a representative sample of measurement for the estimation of the diurnal cycle of evaporation, time series covering a larger period should be considered.
- Seasonal variation of the diurnal cycle of the lake evaporation has to be assessed by taking different seasons of study period.
- Meteorological station must be installed in the lake itself to get a representative data of the lake surface.

LIST OF REFERENCES

- Abreham Kibret, A. (2009). *Open water evaporation estimation using ground measurements and satellite remote sensing : a case study of lake Tana, Ethiopia*. ITC, Enschede. Retrieved from http://www.itc.nl/library/papers_2009/msc/wrem/kibret.pdf
- Ahmed, A. (1999). *Estimation of lake evaporation using meteorological data and remote sensing : a case study of lake Naivasha, central rift valley Kenya*. ITC, Enschede.
- Alcântara, E. H., Stech, J. L., Lorenzzetti, J. A., Bonnet, M. P., Casamitjana, X., Assireu, A. T., & Novo, E. M. L. d. M. (2010). Remote sensing of water surface temperature and heat flux over a tropical hydroelectric reservoir. *Remote Sensing of Environment*, 114(11), 2651-2665. doi: 10.1016/j.rse.2010.06.002
- Alemseged, B. (2010). *Remote sensing of the annual heat storage changes in Lake Tana, Ethiopia*. University of Twente Faculty of Geo-Information and Earth Observation ITC, Enschede.
- Bastiaanssen, W. G. M., Menenti, M., Feddes, R. A., & Holtslag, A. A. M. (1998). A remote sensing surface energy balance algorithm for land (SEBAL) - 1. Formulation. [Article]. *Journal of Hydrology*, 213(1-4), 198-212.
- Bastiaanssen, W. G. M., Pelgrum, H., Wang, J., Ma, Y., Moreno, J. F., Roerink, G. J., & van der Wal, T. (1998). A remote sensing surface energy balance algorithm for land (SEBAL) - 2. Validation. [Article]. *Journal of Hydrology*, 213(1-4), 213-229.
- Becker, F., & Li, Z.-L. (1990). Towards a local split window method over land surfaces. *International Journal of Remote Sensing*, 11(3), 369-393. doi: 10.1080/01431169008955028
- Brutsaert, W. (2005). *Hydrology : an introduction*. Cambridge: Cambridge University Press.
- Brutsaert, W., & Sugita, M. (1992). Application of self-preservation in the diurnal evolution of the surface energy budget to determine daily evaporation. *Journal of Geophysical Research*.
- Coll, C., Caselles, V., Sobrino, J. A., & Valor, E. (1994). On the atmospheric dependence of the split-window equation for land surface temperature. *International Journal of Remote Sensing*, 15(1), 105-122. doi: 10.1080/01431169408954054
- Dingman, S. L. (2002). *Physical hydrology* (Second edition ed.). Upper Saddle River: Prentice Hall.
- Eichinger, W. E., Nichols, J., Prueger, J. H., L.E.Hipps, C.M.U, N., Cooper, D. I., & A.S.Bawazir. (2003). *Lake Evaporation Estimation in Arid Environments, Final Report*.
- Gieske, A. S. M., Hendrikse, J., Retsios, V., Leeuwen, B. v., Maathuis, B. H. P., Romaguera, M., . . . Su, Z. (2005). *Processing of MSG-1 SEVIRI data in the thermal infrared - algorithm developement with the use of the SPARC2004 data set*.
- Kebede, S., Travi, Y., Alemayehu, T., & Marc, V. (2006). Water balance of Lake Tana and its sensitivity to fluctuations in rainfall, Blue Nile basin, Ethiopia. *Journal of Hydrology*, 316(1-4), 233-247. doi: 10.1016/j.jhydrol.2005.05.011
- Kimura, F., & Shimizu, Y. (1994). Estimation of Sensible and Latent Heat Fluxes from Soil Surface Temperature Using a Linear Air-Land Heat Transfer Model. *Journal of Applied Meteorology*, 33(4), 477-489. doi: 10.1175/1520-0450(1994)033<0477:eosalh>2.0.co;2
- Liang, S. (2004). *Quantitative remote sensing of land surfaces : also as e-book*. Hoboken etc.: Wiley & Sons.
- Liang, S. L. (2001b). An optimization algorithm for separating land surface temperature and emissivity from multispectral thermal infrared imagery. *IEEE Transactions on Geoscience and Remote Sensing*, 39(2), 264-274.
- Maathuis, B. H. P., Mannaerts, C. M., Schouwenburg, M., Retsios, V., & Lemmens, R. L. G. (2011). *GEONETCast TOOLBOX : Installation, Configuration and User Guide of the GEONETCast TOOLBOX Plug-in for ILWIS 3.7:ITC*, Enschede.
- Maidment, D. R. (1993). *Handbook of hydrology*. New York etc.: McGraw-Hill.
- Murray, T., & Verhoef, A. (2007). Moving towards a more mechanistic approach in the determination of soil heat flux from remote measurements. A universal approach to calculate thermal inertia. *Agricultural and Forest Meteorology* 147 , 80–87, 80–87.
- Parodi, G. N. (2002). *AHVRR Hydrological Analysis System Algorithms and theory - Version 1.3: AHAS algorithms and theory*. Enschede: ITC
- Price, J. C. (1983). Estimating surface temperatures from satellite thermal infrared data--A simple formulation for the atmospheric effect. *Remote Sensing of Environment*, 13(4), 353-361.

- R. J. Granger, & Hedstrom, N. (2011). Modelling hourly rates of evaporation from small lakes. *Hydrology and Earth System Sciences*, 15, 267–277.
- Retsios, B., Hendrikse, J., Gieske, A. S. M., Leeuwen, B. V., & Maathuis, B. (2006). UT-ITC, Enschede, The Netherlands Patent No.
- Rientjes, T. H. M., Perera, B. U. J., Haile, A. T., Reggiani, P., & Muthuwatta, L. P. (2011). Regionalisation for lake level simulation – the case of Lake Tana in the Upper Blue Nile, Ethiopia. *Hydrol. Earth Syst. Sci.*, 15, 1167–1183.
- Román, M. O., Schaaf, C. B., Woodcock, C. E., Strahler, A. H., Yang, X., Braswell, R. H., . . . Wofsy, S. C. (2009). The MODIS (Collection V005) BRDF/albedo product: Assessment of spatial representativeness over forested landscapes. *Remote Sensing of Environment*, 113(11), 2476-2498. doi: 10.1016/j.rse.2009.07.009
- Schmid, J. (2000). The SEVIRI Instrument Retrieved 10/10, 2012, from http://www.eumetsat.int/groups/ops/documents/document/pdf_ten_msg_seviri_instrument.pdf
- Su, Z. (2002). The Surface Energy Balance System (SEBS) for estimation of turbulent heat fluxes. [Article]. *Hydrology and Earth System Sciences*, 6(1), 85-99.
- Sun, D., & Pinker, R. T. (2003). Estimation of land surface temperature from a Geostationary Operational Environmental Satellite (GOES-8). *Journal of geophysical research*, 108(11), 4326. doi: 10.1029/2002JD002422
- Sun, D., & Pinker, R. T. (2007). Retrieval of surface temperature from the MSG-SEVIRI observations: Part I. Methodology. *International Journal of Remote Sensing*, 28(23), 5255-5272. doi: 10.1080/01431160701253246
- Todd, R. W., Evett, S. R., & Howell, T. A. (2000). The Bowen ratio-energy balance method for estimating latent heat flux of irrigated alfalfa evaluated in a semi-arid, advective environment. *Agricultural and Forest Meteorology*, 103(4), 335-348. doi: 10.1016/s0168-1923(00)00139-8
- Vijverberg, J., Sibbing, F. A., & Dejen, E. (2009). Lake Tana: Source of the Blue Nile. The Nile. In H. J. Dumont (Ed.), (Vol. 89, pp. 163-192): Springer Netherlands.
- Wale, A. (2008). *Hydrological balance of Lake Tana upper Blue Nile basin, Ethiopia*. ITC, Enschede. Retrieved from http://www.itc.nl/library/papers_2008/msc/wrem/wale.pdf
- Webster, P. j., Clayson, C. A., & A. Curry, J. (1996). Clouds, Radiation, and Diurnal Cycle of Sea Surface Temperature in the Tropical Western Pacific. *Journal Of Climate*, 9, 1712-1730.
- Xue, Y., & Cracknell, A. P. (1995). Advanced thermal inertia modelling. *International Journal of Remote Sensing*, 16(3), 431-446. doi: 10.1080/01431169508954411

ANEX

Appendix A: ILWIS Script for water surface temperature retrieval

```

ST_151400:=-
29.2629+1.1054*Re_temp_201109151400_band_3+2.2502*(Re_temp_201109151400_band_3-
Re_temp_201109151400_band_4)+0.1322*(Re_temp_201109151400_band_1-
Re_temp_201109151400_band_2)+0.1889*(Re_temp_201109151400_band_3-
Re_temp_201109151400_band_4)^2+464.1204*(1.005694298-1)+5.75*10^-
5*Re_temp_201109151400_band_1*(0.369179083)
ST_151500:=-
29.2629+1.1054*Re_temp_201109151500_band_3+2.2502*(Re_temp_201109151500_band_3-
Re_temp_201109151500_band_4)+0.1322*(Re_temp_201109151500_band_1-
Re_temp_201109151500_band_2)+0.1889*(Re_temp_201109151500_band_3-
Re_temp_201109151500_band_4)^2+464.1204*(1.005694298-1)+5.75*10^-
5*Re_temp_201109151500_band_1*(0.121401564)
ST_160000:=-
20.8035+1.0907*Re_temp_201109160000_band_3+1.8823*(Re_temp_201109160000_band_3-
Re_temp_201109160000_band_4)+0.3357*(Re_temp_201109160000_band_1-
Re_temp_201109160000_band_2)+0.2987*(Re_temp_201109160000_band_3-
Re_temp_201109160000_band_4)^2+350.8949*(1/0.994337944-1)
ST_160400:=-
29.2629+1.1054*Re_temp_201109160400_band_3+2.2502*(Re_temp_201109160400_band_3-
Re_temp_201109160400_band_4)+0.1322*(Re_temp_201109160400_band_1-
Re_temp_201109160400_band_2)+0.1889*(Re_temp_201109160400_band_3-
Re_temp_201109160400_band_4)^2+464.1204*(1.005694298-1)+5.75*10^-
5*Re_temp_201109160400_band_1*(0.157589293)
ST_160900:=-
29.2629+1.1054*Re_temp_201109160900_band_3+2.2502*(Re_temp_201109160900_band_3-
Re_temp_201109160900_band_4)+0.1322*(Re_temp_201109160900_band_1-
Re_temp_201109160900_band_2)+0.1889*(Re_temp_201109160900_band_3-
Re_temp_201109160900_band_4)^2+464.1204*(1.005694298-1)+5.75*10^-
5*Re_temp_201109160900_band_1*(0.982664605)
ST_161200:=-
29.2629+1.1054*Re_temp_201109161200_band_3+2.2502*(Re_temp_201109161200_band_3-
Re_temp_201109161200_band_4)+0.1322*(Re_temp_201109161200_band_1-
Re_temp_201109161200_band_2)+0.1889*(Re_temp_201109161200_band_3-
Re_temp_201109161200_band_4)^2+464.1204*(1.005694298-1)+5.75*10^-
5*Re_temp_201109161200_band_1*(0.774348459)
ST_161400:=-
29.2629+1.1054*Re_temp_201109161400_band_3+2.2502*(Re_temp_201109161400_band_3-
Re_temp_201109161400_band_4)+0.1322*(Re_temp_201109161400_band_1-
Re_temp_201109161400_band_2)+0.1889*(Re_temp_201109161400_band_3-
Re_temp_201109161400_band_4)^2+464.1204*(1.005694298-1)+5.75*10^-
5*Re_temp_201109161400_band_1*(0.366468718)
ST_161500:=-
29.2629+1.1054*Re_temp_201109161500_band_3+2.2502*(Re_temp_201109161500_band_3-

```

$$\text{Re_temp_201109161500_band_4}) + 0.1322 * (\text{Re_temp_201109161500_band_1} - \text{Re_temp_201109161500_band_2}) + 0.1889 * (\text{Re_temp_201109161500_band_3} - \text{Re_temp_201109161500_band_4})^2 + 464.1204 * (1.005694298 - 1) + 5.75 * 10^{-5} * \text{Re_temp_201109161500_band_1} * (0.118507911)$$

Appendix B: ILWIS Script for short wave outgoing

Rso_151500:=dssf_nafr201109151500_res*Alb_257_final
 Rso_151600:=dssf_nafr201109151600_res*Alb_257_final
 Rso_151700:=dssf_nafr201109151700_res*Alb_257_final
 Rso_151800:=dssf_nafr201109151800_res*Alb_257_final
 Rso_151900:=dssf_nafr201109151900_res*Alb_257_final
 Rso_152000:=dssf_nafr201109152000_res*Alb_257_final
 Rso_152100:=dssf_nafr201109152100_res*Alb_257_final
 Rso_152200:=dssf_nafr201109152200_res*Alb_257_final
 Rso_152300:=dssf_nafr201109152300_res*Alb_257_final
 Rso_160000:=dssf_nafr201109160000_res*Alb_257_final
 Rso_160100:=dssf_nafr201109160100_res*Alb_257_final
 Rso_160200:=dssf_nafr201109160200_res*Alb_257_final
 Rso_160300:=dssf_nafr201109160300_res*Alb_257_final
 Rso_160400:=dssf_nafr201109160400_res*Alb_257_final
 Rso_160500:=dssf_nafr201109160500_res*Alb_257_final
 Rso_160600:=dssf_nafr201109160600_res*Alb_257_final
 Rso_160700:=dssf_nafr201109160700_res*Alb_257_final
 Rso_160800:=dssf_nafr201109160800_res*Alb_257_final
 Rso_160900:=dssf_nafr201109160900_res*Alb_257_final
 Rso_161000:=dssf_nafr201109161000_res*Alb_257_final
 Rso_161100:=dssf_nafr201109161100_res*Alb_257_final
 Rso_161200:=dssf_nafr201109161200_res*Alb_257_final
 Rso_161300:=dssf_nafr201109161300_res*Alb_257_final
 Rso_161400:=dssf_nafr201109161400_res*Alb_257_final
 Rso_161500:=dssf_nafr201109161500_res*Alb_257_final

Appendix C: ILWIS Script for outgoing long wave radiation

Rlo_151500:=0.9744*5.67*10^{-8}*WST_151500_CM^4
 Rlo_151600:=0.9744*5.67*10^{-8}*WST_151600_CM^4
 Rlo_151700:=0.9744*5.67*10^{-8}*WST_151700_CM^4
 Rlo_151800:=0.9744*5.67*10^{-8}*WST_151800_CM^4
 Rlo_151900:=0.9744*5.67*10^{-8}*WST_151900_CM^4
 Rlo_152000:=0.9744*5.67*10^{-8}*WST_152000_CM^4
 Rlo_152100:=0.9744*5.67*10^{-8}*WST_152100_CM^4
 Rlo_152200:=0.9744*5.67*10^{-8}*WST_152200_CM^4
 Rlo_152300:=0.9744*5.67*10^{-8}*WST_152300_CM^4
 Rlo_160000:=0.9744*5.67*10^{-8}*WST_160000_CM^4
 Rlo_160100:=0.9744*5.67*10^{-8}*WST_160100_CM^4
 Rlo_160200:=0.9744*5.67*10^{-8}*WST_160200_CM^4

$Rlo_{160300}:=0.9744*5.67*10^{-8}*WST_{160300_CM}^4$
 $Rlo_{160400}:=0.9744*5.67*10^{-8}*WST_{160400_CM}^4$
 $Rlo_{160500}:=0.9744*5.67*10^{-8}*WST_{160500_CM}^4$
 $Rlo_{160600}:=0.9744*5.67*10^{-8}*WST_{160600_CM}^4$
 $Rlo_{160700}:=0.9744*5.67*10^{-8}*WST_{160700_CM}^4$
 $Rlo_{160800}:=0.9744*5.67*10^{-8}*WST_{160800_CM}^4$
 $Rlo_{160900}:=0.9744*5.67*10^{-8}*WST_{160900_CM}^4$
 $Rlo_{161000}:=0.9744*5.67*10^{-8}*WST_{161000_CM}^4$
 $Rlo_{161100}:=0.9744*5.67*10^{-8}*WST_{161100_CM}^4$
 $Rlo_{161200}:=0.9744*5.67*10^{-8}*WST_{161200_CM}^4$
 $Rlo_{161300}:=0.9744*5.67*10^{-8}*WST_{161300_CM}^4$
 $Rlo_{161400}:=0.9744*5.67*10^{-8}*WST_{161400_CM}^4$
 $Rlo_{161500}:=0.9744*5.67*10^{-8}*WST_{161500_CM}^4$

Appendix D: ILWIS Script for Net radiation

$Rnet_{151500}:=Rs_{net_{151500}}+Rl_{net_{151500}}$
 $Rnet_{151600}:=Rs_{net_{151600}}+Rl_{net_{151600}}$
 $Rnet_{151700}:=Rs_{net_{151700}}+Rl_{net_{151700}}$
 $Rnet_{151800}:=Rs_{net_{151800}}+Rl_{net_{151800}}$
 $Rnet_{151900}:=Rs_{net_{151900}}+Rl_{net_{151900}}$
 $Rnet_{152000}:=Rs_{net_{152000}}+Rl_{net_{152000}}$
 $Rnet_{152100}:=Rs_{net_{152100}}+Rl_{net_{152100}}$
 $Rnet_{152200}:=Rs_{net_{152200}}+Rl_{net_{152200}}$
 $Rnet_{152300}:=Rs_{net_{152300}}+Rl_{net_{152300}}$
 $Rnet_{160000}:=Rs_{net_{160000}}+Rl_{net_{160000}}$
 $Rnet_{160100}:=Rs_{net_{160100}}+Rl_{net_{160100}}$
 $Rnet_{160200}:=Rs_{net_{160200}}+Rl_{net_{160200}}$
 $Rnet_{160300}:=Rs_{net_{160300}}+Rl_{net_{160300}}$
 $Rnet_{160400}:=Rs_{net_{160400}}+Rl_{net_{160400}}$
 $Rnet_{160500}:=Rs_{net_{160500}}+Rl_{net_{160500}}$
 $Rnet_{160600}:=Rs_{net_{160600}}+Rl_{net_{160600}}$
 $Rnet_{160700}:=Rs_{net_{160700}}+Rl_{net_{160700}}$
 $Rnet_{160800}:=Rs_{net_{160800}}+Rl_{net_{160800}}$
 $Rnet_{160900}:=Rs_{net_{160900}}+Rl_{net_{160900}}$
 $Rnet_{161000}:=Rs_{net_{161000}}+Rl_{net_{161000}}$
 $Rnet_{161100}:=Rs_{net_{161100}}+Rl_{net_{161100}}$
 $Rnet_{161200}:=Rs_{net_{161200}}+Rl_{net_{161200}}$
 $Rnet_{161300}:=Rs_{net_{161300}}+Rl_{net_{161300}}$
 $Rnet_{161400}:=Rs_{net_{161400}}+Rl_{net_{161400}}$

Appendix E: ILWIS Script for Latent heat flux

$LE_{flux_{151500}}:=(Rnet_{151500}-(-151.771))/(1+0.163640648)$
 $LE_{flux_{151600}}:=(Rnet_{151600}-(2.882309))/(1+0.222808259)$
 $LE_{flux_{151700}}:=(Rnet_{151700}-(-11.2698))/(1+0.269333253)$
 $LE_{flux_{151800}}:=(Rnet_{151800}-(-83.9595))/(1+0.316654558)$

LE_flux_151900:=(Rnet_151900-(-87.9452))/(1+0.331040144)
LE_flux_152000:=(Rnet_152000-(-64.9983))/(1+0.33569766)
LE_flux_152100:=(Rnet_152100-(-49.3355))/(1+0.331645713)
LE_flux_152200:=(Rnet_152200-(-37.9918))/(1+0.31265426)
LE_flux_152300:=(Rnet_152300-(-44.9625))/(1+0.316703342)
LE_flux_160000:=(Rnet_160000-(-24.2084))/(1+0.337079508)
LE_flux_160100:=(Rnet_160100-(-13.031))/(1+0.359641615)
LE_flux_160200:=(Rnet_160200-(-69.5642))/(1+0.368315973)
LE_flux_160300:=(Rnet_160300-(-0.44934))/(1+0.377387044)
LE_flux_160400:=(Rnet_160400-(0))/(1+0.347150415)
LE_flux_160500:=(Rnet_160500-(0.786353))/(1+0.295503278)
LE_flux_160600:=(Rnet_160600-(8.35648))/(1+0.216499972)
LE_flux_160700:=(Rnet_160700-(49.64371))/(1+0.166998198)
LE_flux_160800:=(Rnet_160800-(107.3055))/(1+0.143368798)
LE_flux_160900:=(Rnet_160900-(338.6461))/(1+0.127363779)
LE_flux_161000:=(Rnet_161000-(-9.99492))/(1+0.122115026)
LE_flux_161100:=(Rnet_161100-(10.25363))/(1+0.093313643)
LE_flux_161200:=(Rnet_161200-(48.87658))/(1+0.137860633)
LE_flux_161300:=(Rnet_161300-(20.13626))/(1+0.109621827)
LE_flux_161400:=(Rnet_161400-(-8.604))/(1+0.079240082)

Appendix F: ILWIS Script for hourly evaporation

Evapo_151500:=LE_flux_151500*3600/(2450000)
Evapo_151600:=LE_flux_151600*3600/(2450000)
Evapo_151700:=LE_flux_151700*3600/(2450000)
Evapo_151800:=LE_flux_151800*3600/(2450000)
Evapo_151900:=LE_flux_151900*3600/(2450000)
Evapo_152000:=LE_flux_152000*3600/(2450000)
Evapo_152100:=LE_flux_152100*3600/(2450000)
Evapo_152200:=LE_flux_152200*3600/(2450000)
Evapo_152300:=LE_flux_152300*3600/(2450000)
Evapo_160000:=LE_flux_160000*3600/(2450000)
Evapo_160100:=LE_flux_160100*3600/(2450000)
Evapo_160200:=LE_flux_160200*3600/(2450000)
Evapo_160300:=LE_flux_160300*3600/(2450000)
Evapo_160400:=LE_flux_160400*3600/(2450000)
Evapo_160500:=LE_flux_160500*3600/(2450000)
Evapo_160600:=LE_flux_160600*3600/(2450000)
Evapo_160700:=LE_flux_160700*3600/(2450000)
Evapo_160800:=LE_flux_160800*3600/(2450000)
Evapo_160900:=LE_flux_160900*3600/(2450000)
Evapo_161000:=LE_flux_161000*3600/(2450000)
Evapo_161100:=LE_flux_161100*3600/(2450000)
Evapo_161200:=LE_flux_161200*3600/(2450000)
Evapo_161300:=LE_flux_161300*3600/(2450000)
Evapo_161400:=LE_flux_161400*3600/(2450000)

Appendix G: ILWIS Script for Daily Total evaporation

Evapo_Total:=Evapo_151500_Tana1+Evapo_151600_Tana+Evapo_151700_Tana+Evapo_151800_Tana+Evapo_151900_Tana+Evapo_152000_Tana+Evapo_152100_Tana+Evapo_152200_Tana+Evapo_152300_Tana+Evapo_160000_Tana+Evapo_160100_Tana+Evapo_160200_Tana+Evapo_160300_Tana+Evapo_160400_Tana1+Evapo_160500_Tana+Evapo_160600_Tana+Evapo_160700_Tana+Evapo_160800_Tana+Evapo_160900_Tana+Evapo_161000_Tana+Evapo_161100_Tana+Evapo_161200_Tana+Evapo_161300_Tana+Evapo_161400_Tana

Appendix H: Hourly estimate of the component of energy balance(in situ)

DOY	Sensible heat flux	NET RADIATION	WATER FLUX	HEAT
258.71	16.80343319	57.89508138		
258.75	74.34172832	-29.61119899	-151.7711215	
258.79	43.33499586	-71.12087426	2.882309322	
258.83	56.88368742	-87.47179712	-11.26982945	
258.88	44.50754269	-79.5167663	-83.95945339	
258.92	12.04531042	-67.66781588	-87.94516984	
258.96	5.154825345	-60.78524891	-64.99829237	
259.00	11.31082752	-65.76258884	-49.3355279	
259.04	17.38853239	-73.50969789	-37.99179308	
259.08	7.805938245	-72.23601176	-44.96254732	
259.13	11.51048955	-79.70682492	-24.20844209	
259.17	13.24376542	-77.45993477	-13.03099435	
259.21	13.52154944	-74.95112201	-69.56416596	
259.25	12.33229351	-67.06439709	-0.449344633	
259.29	9.466220394	-39.18297707	0	
259.33	15.57236908	66.19124433	0.786353107	
259.38	13.3657127	293.0556374	8.356479873	
259.42	10.44433781	637.4923808	49.64371328	
259.46	20.43954712	742.2342783	107.3054603	
259.50	22.66817338	783.7680081	338.6461348	
259.54	22.40874776	510.6591344	-9.994919681	
259.58	11.3859647	302.6533099	10.25363065	
259.63	24.33113048	278.7660633	48.87657556	
259.67	19.4672714	185.6536646	20.13625636	

Appendix I: Latent heat flux estimated by four methods (in situ)

DOY	LE=H/Bo	LE=(Rn-G)/(1+Bo)	LE=Rn-H-G	Penman
258.71	157.0042	-	-	-
258.75	454.2987	104.9808	47.81819	95.77212
258.79	194.4946	-60.519	-117.338	-57.7187
258.83	211.2019	-60.0331	-133.086	-60.1665
258.88	140.5555	3.374224	-40.0649	3.420044
258.92	36.38625	15.23422	8.232044	15.17275
258.96	15.35556	3.154189	-0.94178	3.109589
259.00	34.10515	-12.3359	-27.7379	-12.2499
259.04	55.61585	-27.0581	-52.9064	-26.7511
259.08	24.64748	-20.7134	-35.0794	-20.6744
259.13	34.1477	-41.5072	-67.0089	-42.2043
259.17	36.8249	-47.3867	-77.6727	-48.2124
259.21	36.71182	-3.93692	-18.9085	-4.03136
259.25	32.67811	-48.3634	-78.9473	-49.3475
259.29	27.26835	-29.0858	-48.6492	-29.4172
259.33	52.69779	50.48609	49.83252	49.72858
259.38	61.7354	234.0314	271.3334	216.4056
259.42	62.54162	503.7271	577.4043	452.2505
259.46	142.5662	555.3141	614.4893	491.2901
259.50	177.9797	394.8343	422.4537	346.384
259.54	183.5052	463.9935	498.2453	406.29
259.58	122.0182	267.4435	281.0137	225.5377
259.63	176.4908	202.0366	205.5584	182.3328
259.67	177.5857	149.1656	146.0501	130.9208

Appendix J: Comparison of hourly results

DOY	Net Radiation		Sensible heat		Water heat	Latent heat		Evaporation	
	RS	In situ	RS	In situ	In situ	RS	In situ	RS	In situ
258.75	-66.34	-29.61	11.87	74.34	-151.77	72.56	104.98	0.11	0.15
258.79	-69.34	-71.12	-13.16	43.33	2.88	-59.06	-60.52	-0.09	-0.09
258.83	-72.34	-87.47	-12.96	56.88	-11.27	-48.11	-60.03	-0.07	-0.09
258.88	-75.34	-79.52	2.07	44.51	-83.96	6.55	3.37	0.01	0.00
258.92	-76.34	-67.67	2.64	12.05	-87.95	7.97	15.23	0.01	0.02
258.96	-97.34	-60.79	-8.38	5.15	-65.00	-24.96	3.15	-0.04	0.00
259.00	-79.34	-65.76	-7.72	11.31	-49.34	-23.28	-12.34	-0.03	-0.02
259.04	-81.34	-73.51	-1.50	17.39	-37.99	-4.79	-27.06	-0.01	-0.04
259.08	-90.91	-72.24	-7.13	7.81	-44.96	-22.52	-20.71	-0.03	-0.03
259.13	-113.87	-79.71	-8.93	11.51	-24.21	-26.50	-41.51	-0.04	-0.06
259.17	-97.02	-77.46	-12.24	13.24	-13.03	-34.04	-47.39	-0.05	-0.07
259.21	-98.69	-74.95	3.45	13.52	-69.56	9.37	-3.94	0.01	-0.01
259.25	-115.17	-67.06	-15.95	12.33	-0.45	-42.25	-48.36	-0.06	-0.07
259.29	-84.34	-39.18	-21.74	9.47	0.00	-62.60	-29.09	-0.09	-0.04
259.33	-5.64	66.19	-12.17	15.57	0.79	-41.19	50.49	-0.06	0.07
259.38	514.03	293.06	77.92	13.37	8.36	359.88	234.03	0.53	0.34
259.42	666.88	637.49	87.77	10.44	49.64	525.58	503.73	0.77	0.74
259.46	785.15	742.23	81.82	20.44	107.31	570.67	555.31	0.84	0.82
259.50	847.29	783.77	57.76	22.67	338.65	453.45	394.83	0.67	0.58
259.54	722.71	510.66	95.43	22.41	-9.99	781.48	463.99	1.15	0.68
259.58	769.99	302.65	53.85	11.39	10.25	577.08	267.44	0.85	0.39
259.63	296.86	278.77	47.19	24.33	48.88	342.31	202.04	0.50	0.30
259.67	424.78	185.65	34.62	19.47	20.14	315.77	149.17	0.46	0.22
259.71	193.77	45.16	7.92	10.97	36.30	99.94	41.84	0.15	0.06